IOTC–2017–WPTT19–20
Received: 21 September

The Dynamic Simulation of Pelagic Longline Retrieving

Liming Song[a, b, c,d*], Zhibin Shen[a], Jie Li[a], Xinfeng Zhang[a, b, c,d]

a College of Marine Sciences, Shanghai Ocean University, 999 Huchenghuan Road, Lingangxincheng Shanghai 201306, China

b National Engineering Research Centre for Oceanic Fisheries, Shanghai Ocean University, 999 Huchenghuan Road, Lingangxincheng Shanghai 201306, China;

c Key Laboratory of Sustainable Exploitation of Oceanic Fisheries Resources (Shanghai Ocean University), Ministry of Education, 999 Huchenghuan Road, Lingangxincheng Shanghai 201306, China

d Collaboration Innovation Center for National Distant-water Fisheries, Shanghai 201306, China

*Corresponding author: Liming Song, Tel.: +86 21 61900311; Fax: +86 21 61900304.
E-mail addresses: lmsong@shou.edu.cn (Liming Song)

Abstract: It is important to understand the interactions among sea current, fishing vessel, line hauler, and catches during the pelagic longline gear retrieving for improving fishing gear performance and efficiency. In this study, fishing gear configuration parameters, operational parameters and three-dimensional (3D) ocean current data were collected in the Indian Ocean. Dynamic models of pelagic longline gear retrieving were built using the lumped mass method, and solved using the Euler-Trapezoidal method. The results are: (1) pulling force of line hauler exerted on the gear was 2800N～3600N; (2) there were no significant differences ($P > 0.05$) between the time of the hook retrieving measured at sea and that of simulated; and (3) the absolute value of moving velocity at representative nodes along the X, Y and Z axes was 0.01～25.5m/s. These results suggest that the dynamic model of longline fishing gear retrieving could be used: (1) to understand the interaction among the sea current, fishing vessel, line hauler, longline gear and the catches; (2) to provide basic data for optimizing the design of the line hauler; and (3) to serve as a reference to study the hydrodynamic performance of other fishing gears during the hauling process.

Key words: pelagic longline; retrieving; dynamic simulation; visualization

1. Introduction

Pelagic longline belongs to multi-body system. There are interconnections between the structure and fluid, and the interference among structure in the multi-body system in the fluid (Zhou et al., 2001). The hook depth of pelagic longline is a key parameter, and understanding the hook depth of pelagic longline is important to reduce bycatch and protect the biodiversity (Song et al., 2015). There were many studies on pelagic longline gear hydrodynamic performance, line shape, tension distribution, and hook depth during the deployment process (Suzuki et al., 1977; Boggs, 1992; Bigelow et al., 2002; Song et al., 2015). The methodology to study the pelagic longline gear hydrodynamic performance can be summarized as the theoretical calculation, measurement at sea, and the integration of numerical simulation, model test in flume tank and measurement at sea. These approaches are detailed below.

Theoretical calculation: Some scholars considered the shape of pelagic longline gear as a catenary (Suzuki et al., 1977; Nakano et al., 1997; Song et al., 2004; Jiang et al., 2005). Wu and Wu (2005) considered the shape of pelagic longline gear as a simple parabola under the water. In fact, the shape of pelagic longline gear influenced by various factors under the water, the force and shape changed greatly with different current. There is bias to calculate the hook depth considering the shape of pelagic longline gear as a simple catenary or parabola under the water.

Measurement at sea: Boggs (1992) assumed the current shear between the surface and the thermocline as the main factor affecting hook depth. Mizuno et al. (1998, 1999) studied the fluctuation of longline's shortening rate and its impact on longline underwater shape, and the temperature-depth recorders were used to measure the depth of hooks and the underwater shape of longline gear. Bigelow et al. (2002, 2006) derived an equation for calculating the depth of hooks with different surface currents based on the actually measured hook depth data from Japanese fishing operations in the Pacific Ocean by logistic regression. In addition, the authors studied the relationship between the hook depth and environmental variables, including wind, and current shear, by using generalized linear models (GLM) and generalized additive

models (GAM). Miyamoto et al. (2006) measured the three-dimensional (3D) underwater shape of longline by acoustic positioning system and ORBCOMM float system in the field experiment. Considering the influence of the drift velocity of the gear or current shear, leeway and drift angle, wind speed, wind direction, and relative bearing of apparent wind, Song and Gao (2006) and Song et al. (2008, 2012) applied the stepwise regression method and GLM to study the relationship between actual hook depth and theoretical hook depth, and the prediction hook depth model was developed.

The integration of numerical simulation, model test in flume tank and measurement at sea: There were many studies about the numerical simulation of longline gear. Wan et al. (2002) developed a nonlinear mixed finite element method (FEM) to predict the shape and tension of longline gear. Wan et al. (2005) studied the operation status of longline gear by numerical simulation. Lee et al. (2005) applied the dynamic numerical simulation method for studying the longline gear and used Newmark β method to solve the equations. The results were verified by testing in a flume tank. Song (2008, 2015) and Song et al.(2011a, 2011b) developed the 3D statics model of longline gear deployment by using FEM and verified the model based on the measured hook depth, and 3D current data. Zhang et al. (2012) applied fully implicit algorithm and virtual neural lattice to solve longline mechanical model by using R language programming to obtain the stable solution of the state of equilibrium. This method had higher efficiency and precision to solve complex engineering longline equations. Based on FEM, Cao (2011) built a 3D dynamic model of longline gear and solved the 2^{nd} order differential equations by FEM and implicit Euler method in R language. Cao et al. (2014) built a 3D statics model of pelagic longline and studied the cylinders drag coefficient (C_{N90}) of main line using the principles of static mechanical and FEM. Song et al. (2015) built the dynamic equations of pelagic longline gear deployment using the lumped mass method and taking into account the hydrodynamic force of longline fishing gear floats. These dynamic equations were solved by the Euler-Trapezoidal method and then verified by the field measured data.

At present, there might be few studies on hydrodynamic performance of longline

gear during the process of retrieving. In the present study, the pelagic longline gear retrieving process is simulated by developing dynamic models using the lumped mass method and taking into account the interactions among the sea current, fishing vessel, line hauler, longline gear and catches. The model results can improve our understanding of interactions among sea current, fishing vessel, line hauler, longline gear and the catches, and the dynamic process of the retrieving.

2. Materials and Methods

2.1 Measurements at Sea

2.1.1 Survey vessel, locations, and duration

The survey vessel was the longliner "Xinshiji No. 85". Specifications of the vessel are: overall length 56.50m, molded breadth 8.50m, moulded depth 3.65m, main engine power 735.00kW, and the maximum speed 11.5 kn. The survey duration was from Nov. 18, 2012 through Mar. 31, 2013. The survey area was defined as 2°13'S ~ 8°09'S, 61°49'E ~ 68°16'E (Fig. 1). The data collected from four sites were used to evaluate and verify the simulation model developed in this study.

2.1.2 Fishing gear and methods

The longline gear configuration included 360 mm diameter hard plastic floats, 4.5 mm diameter nylon float line, and a 35 m length, 6.5 mm diameter multifilament main line. The first section of the branch line was made of 4.0 mm diameter polypropylene, and was 2.0 m long. The second section was made of 2.5 mm diameter monofilament and was 19 m long. The third section was made of 2.5 mm diameter lead centred rope and was 3 m long. The fourth section was made of 2.0 mm diameter monofilament and was 13 m long. The fifth section was made of 2.5 mm diameter lead centred rope and was 3 m long. The sixth section was made of 1.3 mm diameter monofilament and was 8 m long. The hanging buckle was connected to the first section by a swivel. The sixth section was directly connected to the hook. The overall length of branch line was about 48 m. Parts of longline gear and assumed parameter of catch were shown in Table 1. There were 16 hooks between floats (Fig. 2).

The longline gear deployments occurred from about 06:00 to 11:30 (local time),

and soak times lasted for about 5.5 hours. The gear was retrieved from about 13:00 to 04:00 of the next day, with the hauling phase lasting for about 15 hours. During the setting operation, the line shooter speed was at about 6.7 m/s and the vessel speed was at approximately 5.2 m/s. The time interval between deploying the fore and after branch lines was approximately 7.4 s. The total hooks per set ranged from 1424 to 3504 hooks.

2.1.3 Survey instruments, method and content

The survey instruments were an Acoustic Doppler Current Profilers (Aquadopp 2000, NORTECK Co., Vangkroken, Norway) and Depth Recorders (DR-1050, RBR Co., Ottawa, Canada). The depths of hook were measured by 10 DRs. The ADCP was used to measure 3D current data at different depths. The depth measurement errors of DRs and ADCP were described in Song et al. (2015). The survey method and content were also described in Song et al. (2015).

2.2 Development of the Numerical Model and Solving Methods

The development of the numerical model and methods in solving the equations are detailed in Song et al. (2015) and as follows.

2.2.1 Basic assumptions

1) The tensile force on the fishing gear between two floats was assumed to be a constant as the line hauler heaving the lines;

2) The wring tension was assumed to act on the node of the connected point between float line and main line (main node) at the beginning, the wring tension acted on the first main line node when the main node retrieved on deck (the node's position in the Z direction under the action of the wring tension was greater than zero), and the main node no longer acted on by the wring tension; the first main line node acted on by the wring tension at that time, the rest could be done as the same manner, wring tension acted on the next node constantly until the whole gear retrieved on the deck (the position of all nodes in the Z direction were greater than zero);

3) The angle between the course of fishing vessel and the direction of fishing gear is about 30° while retrieving. The average speed of fishing vessel was about 2.5 m/s. Considering the influence of fishing vessels' movement during the retrieving

process, the movement speed of fishing vessel was decomposed into two parts, one was along the direction of the connecting line between the two floats (X axis) and the other was along the direction perpendicular to the X axis (Y axis).

2.2.2 Establishment of coordinate system

In the present study, the dynamics occurring between two floats was the basis of the investigation. Because retrieving process simulation was based on the results of deployment process simulation, in this study, the coordinate system was established as the same as that of Song et al. (2015) (Fig. 2).

2.2.3 The tension analysis and the determination of C_m

Pelagic longline gear was composed of four parts, e.g., float, float line, main line and branch line. The major forces on each bar element were as follows (Cao et al., 2014; Song et al., 2015):

The key to simulate the retrieving process of fishing gear is to determine the wring tension acting on bar elements by the line hauler. The tension of main line was not measured by instrument during the retrieving. In this study, the following processing was conducted in order to obtain the wring tension to agree with the retrieving process simulation:

1) The wring tension of line hauler acting on fishing gear was assumed to be a constant;

2) Based on the float line's tension in the initial retrieving status, a certain wring tension was defined and used to simulate the retrieving process. The wring tension would be increased in the step of 100N until wring tension was enough to retrieve the longline gear. The wring tension at this moment was determined as the wring tension acted on the main line during the retrieving process.

2.3 Analysis of each node's space position, speed and tension during retrieving

The space position, speed and tension of all nodes during the retrieving were the key points of this study. The time of initial position of fishing gear was marked as "t = Time 0". The time while the main node (1, 2) retrieved on deck was marked as "t = Time 1", and the time while the main node (1, 3) retrieved on deck was marked as "t = Time 2", and the rest could be done as the same manner, the time while the main node

(1, 19) retrieved on deck was marked as "t=Time 18". The space shape of fishing gear and the space position of each node were studied in the above marked time. The variations of tension and movement speed of all nodes were analyzed from the beginning to the end of retrieving.

Due to a large number of nodes in the model, in this study, the representative nodes were selected to study the fluctuation of space position, movement speed, tension and hydrodynamic force of the nodes, and the representative nodes were the main line node (1, 3), the deepest node (1, 10), and its corresponding branch line node (2, 10). Because the main node (1, 2) was retrieved on the deck by manpower at the beginning of retrieving, the main line node (1, 3) was selected as one of the representative nodes.

2.4 The effects of catches on space position, speed and tension of the corresponding node

In order to make the simulation result of retrieving consistent with the actual situation, in the present study, the scenario with catch was simulated during the retrieving. During the survey, the average weight of fish was 40 kg, and the weight in water was 37.0 N (the formula of weight in water was calculated by $G_s = (\rho_{tuna} - \rho_w) gv$, the density of tuna catch was assumed to be 1.10 g/cm^3, and the catches were assumed to be in dead). It was assumed there were four kinds of situations: node (2, 8) with the catch; nodes (2, 7), (2, 8), and (2, 9) with the catches; nodes (2, 13) with the catch; and nodes (2, 12), (2, 13), and (2, 14) with the catches. Above assumptions can be used to analyze the impacts of different catch distributions on the tension distribution and movement speed of the corresponding node and the whole fishing gear.

2.5 The validation of model

The average retrieving time of each hook and each float was measured and simulated for the selected representative four days (on Dec. 13, 19, 23, and 31, 2012). Wilcoxon rank test (Wilcoxon, 1945) was used to test significant differences between the hook retrieving time measured at sea and the simulated hook retrieving time in

these days. The validation and effectiveness of the model was verified if there was no significant difference between them.

3. Results

3.1 The initial position and velocity of the retrieving process

The initial positions on Dec. 13, 19, 23 and 31, 2012 were shown in Fig.3. The initial velocity of the main nodes, main line nodes and branch line nodes were shown in Fig. 4. The velocity of pelagic longline gear at the steady state was small (Fig. 4). The maximum initial velocity of all nodes in three directions at the steady state of the four days did not exceed 0.08m/s.

3.2 Determine the value of wring tension

Float line suffered the biggest tension when it was in the initial position of the retrieving on Dec. 13, 19, 23 and 31, 2012. The biggest tensions were 258.4N, 271.1N, 251.23N and 259.51N, respectively. Based on the biggest tension of the float line in the initial retrieving state, the initial wring tension was assumed to be 300N at first. This initial wring tension was used to simulate the retrieving process. The wring tension increased in the step of 100N until wring tension was enough to retrieve the longline gear. At last, the wring tension acted on the main line during the retrieving process for Dec. 13, 19, 23 and 31, 2012 was determined as 2800N, 3600N, 3000N and 3500N.

3.3 Verification of the effectiveness of the model

The average retrieving time (measured and simulated) of each hook and float on Dec. 13, 19, 23, and 31, 2012 was shown in Table 2. There were no significant differences (p = 0.882, Dec. 13; p = 0.388, Dec. 19; p = 0.835, Dec. 23, p = 0.416, Dec. 31) between simulated results and the measured results by Wilcoxon rank test (Wilcoxon, 1945).

3.4 The velocity variation of each node in X, Y, and Z axis

In the present study, the movement velocities of the selected representative nodes during the retrieving simulation were analyzed and the results were shown in Fig. 5.

The selected representative nodes were nodes (1, 3), (1, 19), (1, 10), and (2, 10). The movement velocities of the nodes (1, 3) and (1, 10) were negative in the X axis at the beginning under the action of tension. It changed to positive over the time. The velocity of node (1, 3) in the Z axis decreased gradually and fluctuated in a certain range. The velocity of the main line node (1, 10) in the Z axis increased at first, then fluctuated in a certain range. The velocity of main node (1, 19) remains unchanged in X, and Y axes basically before the external tensile forces (T_w) acted on it and increased significantly after the T_w acted on it. The fluctuation of the velocity in the Z axis was small before the T_w acted on it. The velocity in the Z axis increased after the T_w acted on it, and decreased gradually after reaching the maximum. The velocity of nodes in the Y axis was much smaller than that in the X axis, and the velocity in the Z axis was positive generally. The absolute value of velocity of node (2, 10) was much bigger than that of the node (1, 10) on three directions (Table 3).

3.5 The variation of the fishing gear space shape during the retrieving

The space shape of fishing gear and space position of each node was studied in "t = Time 0", "t = Time 1", "t = Time 2", ……, and "t=Time 18". The variations of tension and movement speed of all nodes were analyzed from the beginning of retrieving to the end of retrieving.

Simulated space shape of fishing gear during the retrieving process was shown in Fig. 6. During the retrieving, the space position change of fishing gear on the left side was more obvious than that of the right side. The radian of the left side of the main line was steep while that of the right side was smooth. The position coordinate of each node on the left side increased gradually while that of right side decreased gradually in the X axis. The position coordinate of all the nodes (except to the nodes (1, 19), or (1, 20)) increased gradually in the Z axis. The position coordinate of main node (1, 19) remain unchanged in X, and Y axes basically before the T_w acted on it and increased gradually after the T_w acted on it. The position coordinate of float in the X

axis was mainly influenced by the sea surface hydrodynamic force before the T_w acted on it, and produce the displacement in the direction same as the surface current. For instance, the float influenced by surface current and produced positive but limited displacement along the X axis. The float produced negative displacement due to the effect of T_w when it drifted a distance along the positive direction of X-axis until the retrieving was in the end. Because the direction of the surface currents in the X-axis was negative, the float drifted along the negative direction of X-axis (Fig. 6).

There was a close relationship between the spatial location fluctuation of each node and the fluctuation of hydrodynamics and tension of each node. The simulated fluctuation of hydrodynamic and tension of each node during the retrieving was shown in Fig. 7. The fluctuation trend of hydrodynamic and tension of the node and bar element was consistent with each other. The hydrodynamics of each node increased while tension increased too. The tension of the float node (1, 20) was large all the time, and its hydrodynamic was small before the T_w acted on it. The range of hydrodynamic force and tension of each node was shown in Table 4.

3.6 The simulation of catch influence to retrieving

The catches were assumed to be in dead, their weight in water was 37.0 N. The node (2, 7) was assumed to be with catch, and the nodes (2, 7), (2, 8) and (2, 9) assumed to be with catches on Dec. 13, and 23. The node (2, 14) was assumed to be with catch, and the nodes (2, 12), (2, 13) and (2, 14) assumed to be with catches on Dec. 19 and 31. In the present study, the space shape of fishing gear with catch was compared with no catch when the node (2, 6) had been retrieved on deck ("t = Time 5") (Fig. 8).

One individual of catch did not have obvious effect on the space shape of longline gear during the retrieving process, but three individuals of catches had certain effect on the space shape of longline gear. The fishing gear with the catch was deeper than that with no catch, but the impact was not obvious (Fig. 8).

The node (2, 7) on Dec. 13, 23 and node (2, 14) on Dec. 19, 31 were selected to study the influence of the catches to the velocity of node (Fig. 9). The velocity of

nodes (2, 7) and (2, 14) was large in X, Y, and Z axes, which reflect their smaller mass and bigger tension when there was no catch. The velocity of node (2, 7) and (2, 14) decreased significantly and the fluctuation rang was small when there were catches.

4. Discussion

4.1 The determination of T_w

The wring tensions of main line in four days were determined as 2800N, 3500N, 3600N and 3000N in retrieving the longline gear. These wring tensions were consistent with the actual measurements at sea. The difference of wring tension was large among four days. This might result from the different initial tensions of the fishing gear and the current in four days. Among four days, the initial tension of float line was the biggest on Dec. 19, and the current velocity on Dec. 19 was the greatest. In the case of surface current, the surface current velocity was 0.486 m/s, 0.186 m/s, 0.201 m/s, and 0.360 m/s on Dec.19, 13, 23, and 31, respectively. Larger current produced larger water resistance, and required more tension to retrieve the longline gear. In addition, the tension difference could be also affected by the wind speed. In the present study, the influence of the wind speed was not considered, which should be studied in the future.

In the present study, there were some limitations about the method of determining T_w. T_w was the key factor affecting the result of retrieving simulation of fishing gear. In future, the wring tension acted on the main line by the line hauler should be measured in the field experiment. The actual wring tension can be used to improve the simulation accuracy of pelagic longline gear retrieving.

4.2 Processing of fishing vessel movement during retrieving

The fishing vessel was moving during the retrieving process. Because the angle between the moving direction of the fishing vessel and the fishing gear deployment direction was about 30°, the moving velocity of fishing vessel was decomposed and the retrieving simulation was conducted. This processing method was relatively reasonable, and was consistent with the actual situation.

4.3 The variation of fishing gear space shape, tension and hydrodynamic during the retrieving

The dynamic model of pelagic longline gear retrieving developed in the present study could be used to simulate the retrieving process under all kinds of current. During the retrieving, the velocity of some nodes fluctuated in a certain range. This was resulted from the effect of numerical instability of tension forces between neighbored mass points (Walton and Polachek, 1960; Johansen, 2007; Yao et al., 2016). The space position change of fishing gear on the left side was more obvious than that of the right side. The radian of the left side of the main line was steep while that of the right side was smooth. The reasons might be that the retrieving operation was from left to right, T_w acted on the left node of fishing gear at first and made the corresponding bar element produce elastic deformation, the tensile of elastic deformation affected to the adjoining bar element on the right side, and so on, the more to the right, the smaller the tension. Compared with the left side, the variability of the space position on the right side was smaller, and the radian of main line on the right side was smoother. The position coordinate of each node on the left side increased gradually while that of right side decreased gradually in the X axis. The position coordinate of all the nodes (except to the nodes (1, 19), or (1, 20)) increased gradually in the Z axis. The variation range of the position coordinate of nodes on the left side was bigger than that on the right side. This reflected the situation that the longline gear was heaving. The differences of the position coordinate of nodes between the left side and the right side resulted from the T_w, which acted on the left side of the gear. The position coordinate of float in the X axis was mainly influenced by the sea surface hydrodynamic force before the T_w acted on it, and produce the displacement in the direction same as the surface current. The float influenced by surface current and produced displacement along the X axis. The float produced negative displacement due to the effect of T_w when it drifted a distance along the X-axis until the retrieving was in the end.

The stress of the float was simplified. The impacts of the float line tension and the sea current hydrodynamics on the float were analyzed. The impacts of the wave

and the wind on the float did not take into account. This might result in biases in the simulation of the float movement. In order to improve the model, the impacts of the wave and the wind on the float should be considered in the future.

The forces that the longline gear experienced were extremely complex in the actual operation, including the hydrodynamic forces, gravity, buoyancy, and forces (of the wind, and waves) acted on the float. Because the hydrodynamic forces acted on the branch line, hook and bait, were all extremely complex, the forces acted on the float by the wind and waves, and the hydrodynamic forces on the bait and catch were not taken into account in the model. The present study simplified the hydrodynamic forces of the branch line. Tests should be carried out in a flume tank to better understand the hydrodynamic coefficients of the bait and catch.

There was a close relationship between the spatial location fluctuation of each node and the fluctuation of hydrodynamics and tension of each node. The fluctuation trend of hydrodynamic and tension of the node and bar element was consistent with each other. The hydrodynamics of each node increased while tension increased.

The hydrodynamics of the nodes and bar elements would increase while the wring tension increased. The reason might be that the increased wring tension increased the moving velocity of the nodes.

4.4 The influence of catches to the retrieving

An individual fish in catch did not show obvious effect on the space shape of longline gear during the retrieving process, but three individuals had certain effects. The fishing gear with the catch was deeper than that with no catch, but the impact on the space shape of longline was not obvious (Fig. 8).

The impact of catches on the depth and velocity of the branch line was obvious. The branch line with the catch was deeper than that with no catch. The movement velocity of the corresponding node with the catch had a significant reduction and the variation range was very small. This might result from the mass of branch node with the catch was increased, the more catches, the greater the mass.

The present study simplified the hydrodynamic forces of the branch line. The hydrodynamic forces on the catch were not considered in the model and the catch was

assumed as dead. The mass of the branch line node with the catch increased. The dynamic tension of the catch should be calculated and the moving direction of living catches included into the model in the future study.

5. Conclusions

The dynamic equations of pelagic longline gear retrieving built by lumped mass method could be used to simulate the pelagic longline gear retrieving process and be solved by Euler-Trapezoidal method using R language programming. There were no significant differences between the time of the hook retrieving measured at sea and the time of simulated hook retrieving. During the retrieving, the pulling force of line hauler exerted on the gear was 2800N～3600N, the absolute value of moving velocity at representative nodes along the X, Y and Z axes was in the ranges of 0.01～24.70 m/s, 0.07～25.5m/s, and 0.07～25.1m/s, respectively, and one individual tuna catch didn’t produce significant effect on the shape of the gear, but three individual tuna catch produced certain effect on the configuration of the gear. The dynamic model of longline fishing gear retrieving developed in the present study could be used to understand the interaction among the sea current, fishing vessel, line hauler, longline gear and the catches, to provide basic data for optimizing the design of the line hauler, and to serve as a reference to study the hydrodynamic performance of other fishing gears (eg. trawl and purse seine) during the hauling process.

Acknowledgements

The project is funded by the National High Technology Research and Development Program of China (Project No. 2012AA092302), Specialized Research Fund for the doctoral program of higher education (No. 20113104110004), and the Shanghai Municipal Education Commission Innovation Project (Project No. 12ZZ168). We thank Mr. D C Zheng, F Lin and the crews of longliner "Xinshiji No. 85" of Zhejiang Ocean Family Co., Ltd. for their support. Gratitude also goes to Professor Yong Chen at University of Maine for reviewing the manuscript.

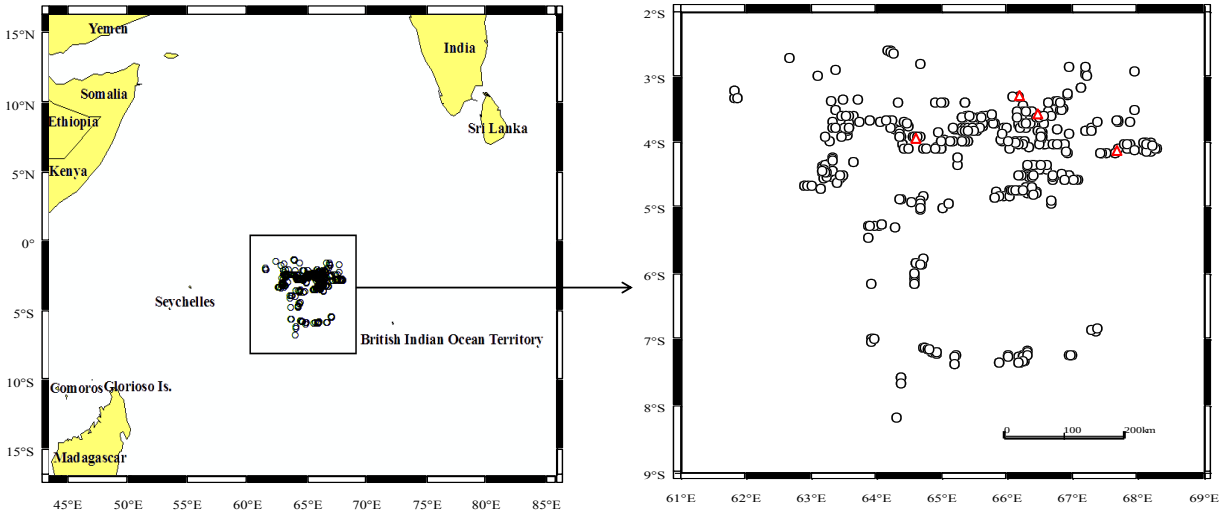

Fig.1. Survey area and sites (○:survey sites, ▵:sites selected to verify the model)

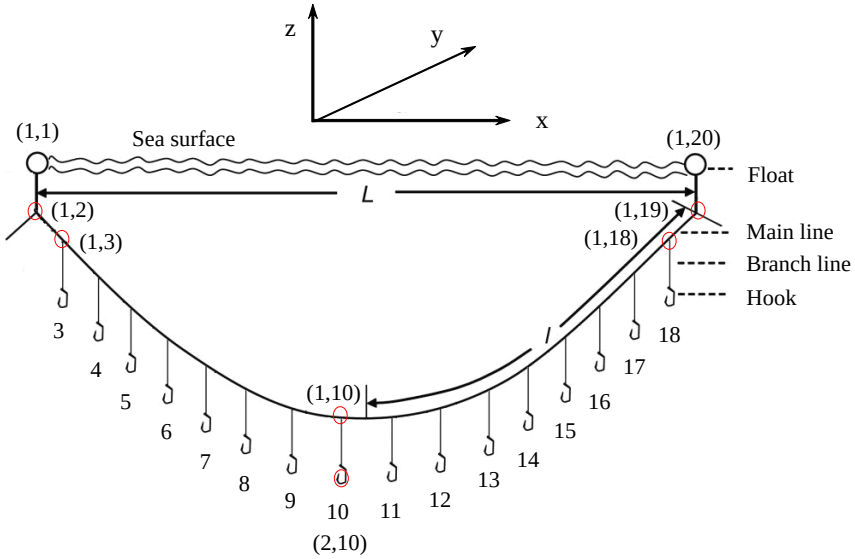

Fig.2 The configuration of pelagic longline and a diagram of the coordinates system for the numerical calculation. XOYZ is the coordinate system. The nodes (1,1), and (1,20) are float nodes. The nodes (1,2), and (1,19) are main nodes and they are the nodes of connected points between float line and main line. The nodes (1,3), (1,10) and (1,18) are main line nodes. The node (2,10) is branch line node. The numbers 3, 4, ……, and, 18 are the numbers of branch line. L is the distance between both floats (m). l is half of the arc length of mainline (m).

(A)

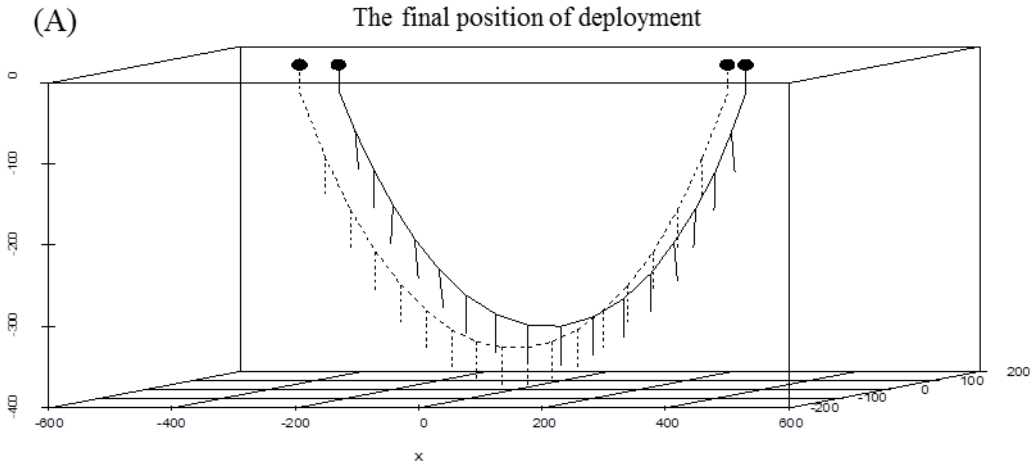

--- The standard catenary —— The final position of deployment

(B)

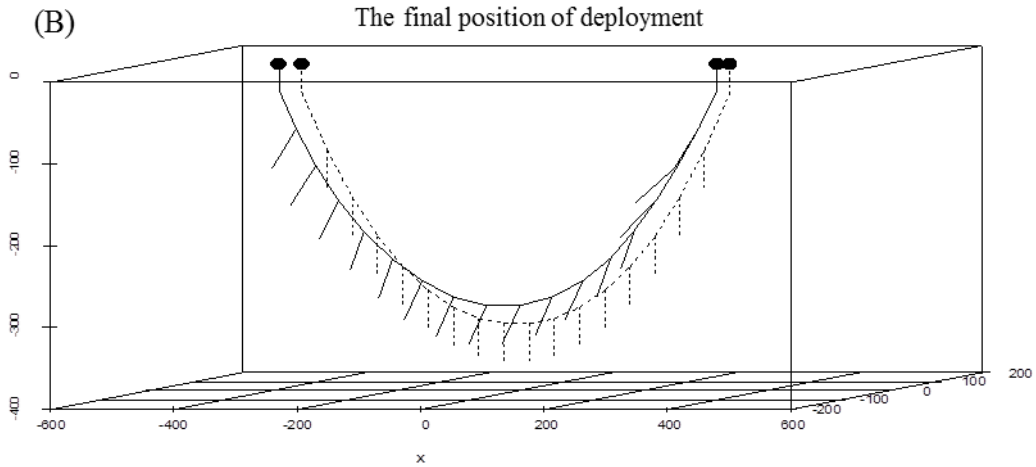

--- The standard catenary —— The final position of deployment

(C)

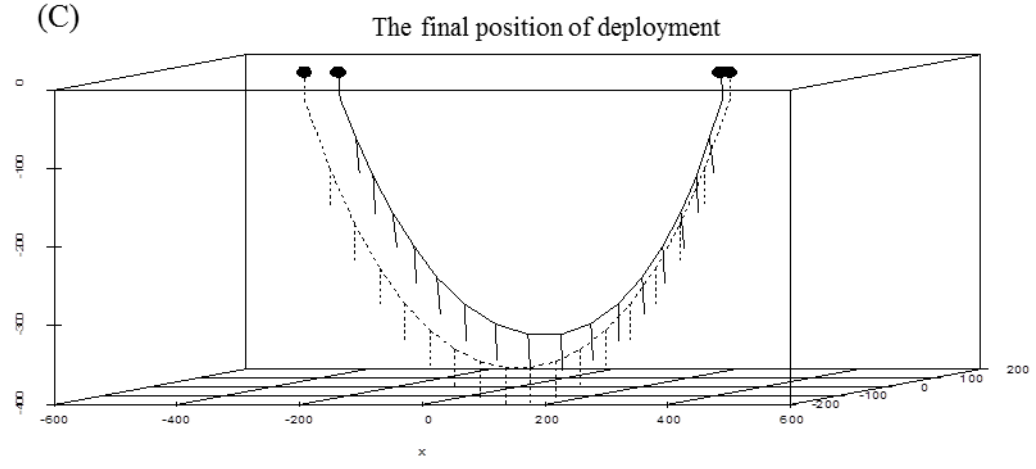

--- The standard catenary —— The final position of deployment

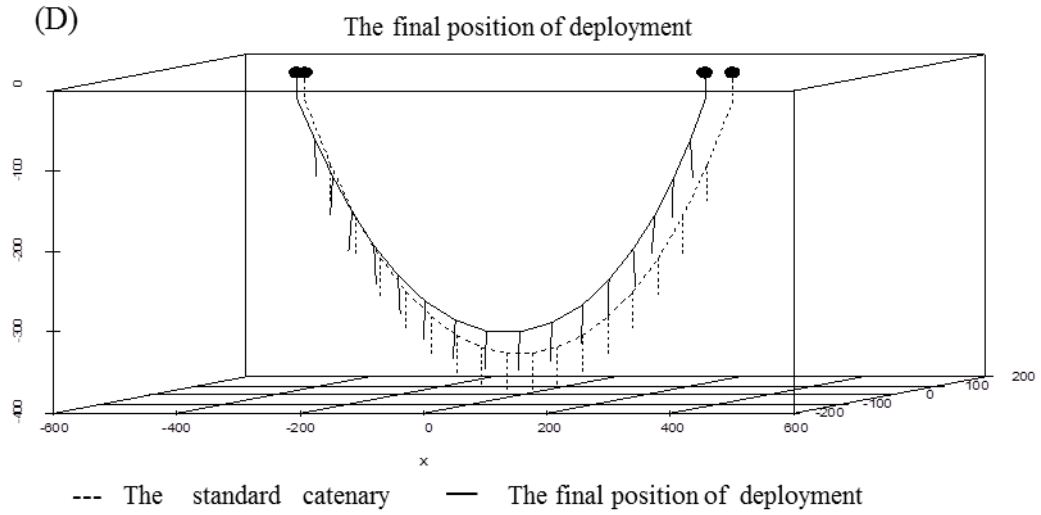

Fig.3 The settlement of longline based on the dynamic model data from survey in 2012
(A: Dec. 13, 2012; B: Dec. 19, 2012; C: Dec. 23, 2012; D: Dec. 31, 2012

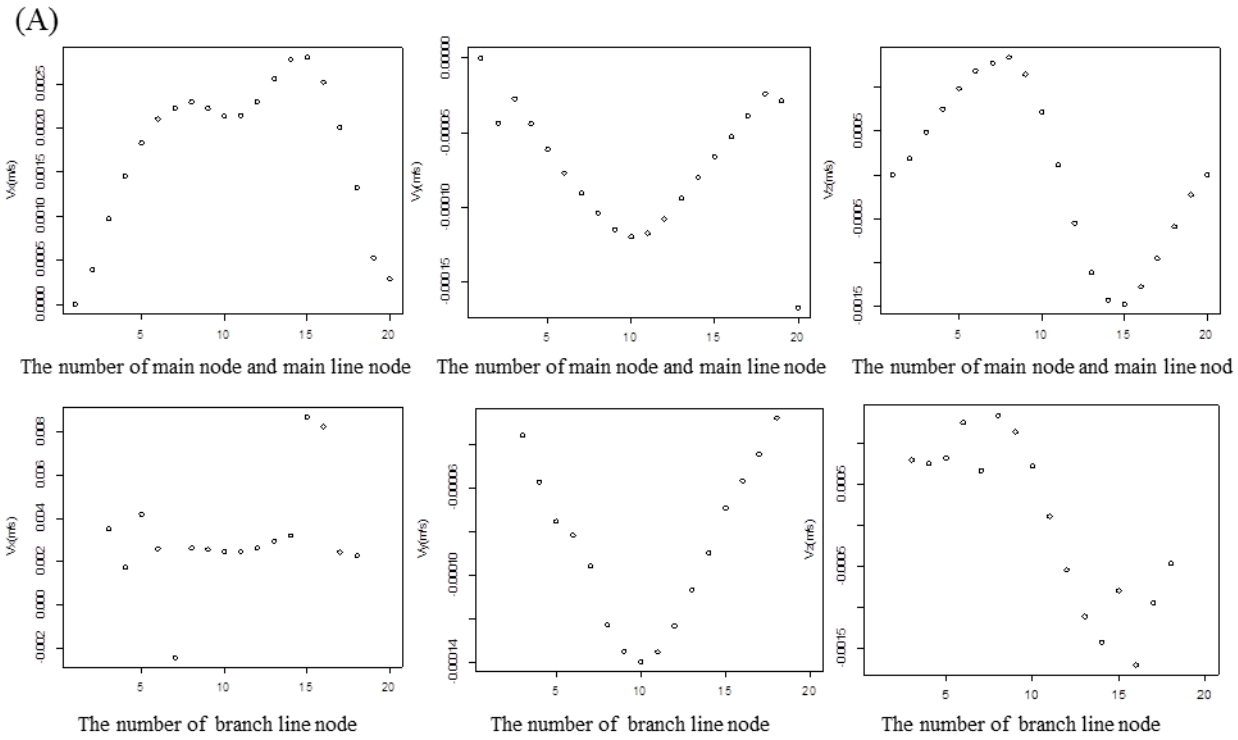

(B)

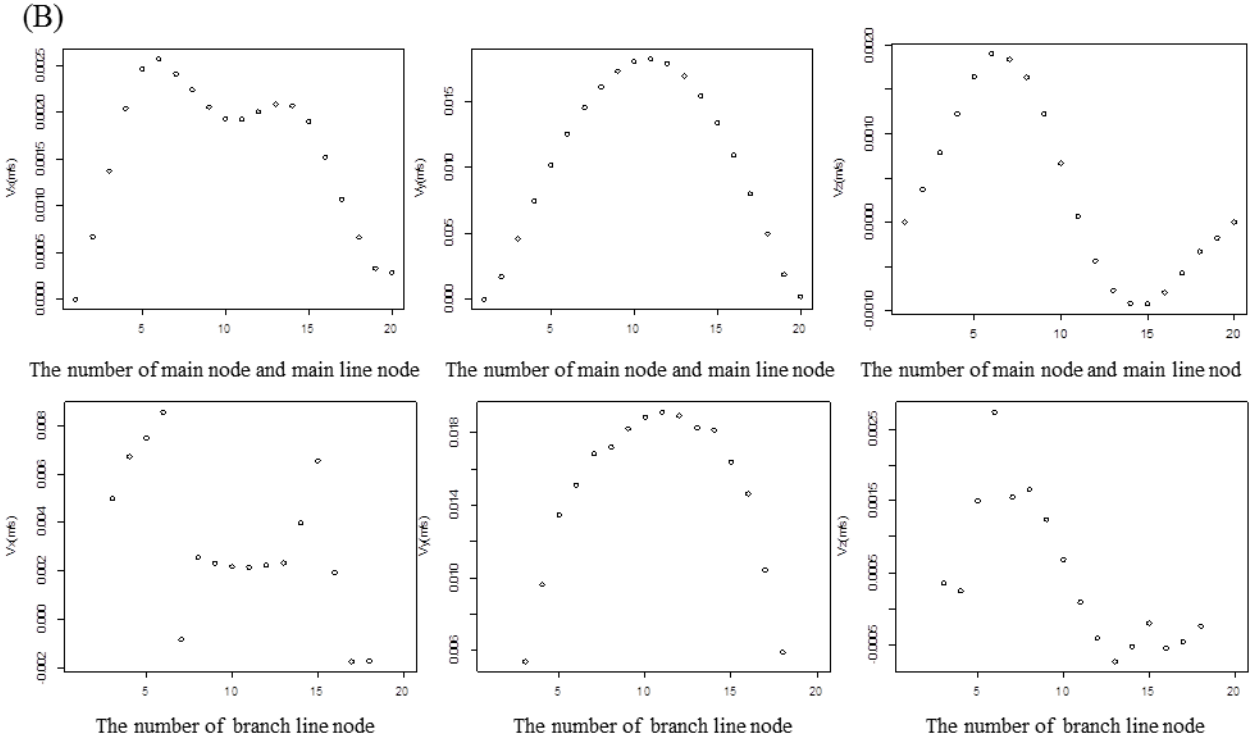
Vx(m/s)
Vy(m/s)
Vz(m/s)
The number of main node and main line node
The number of main node and main line node
The number of main node and main line nod
The number of branch line node
The number of branch line node
The number of branch line node

(C)

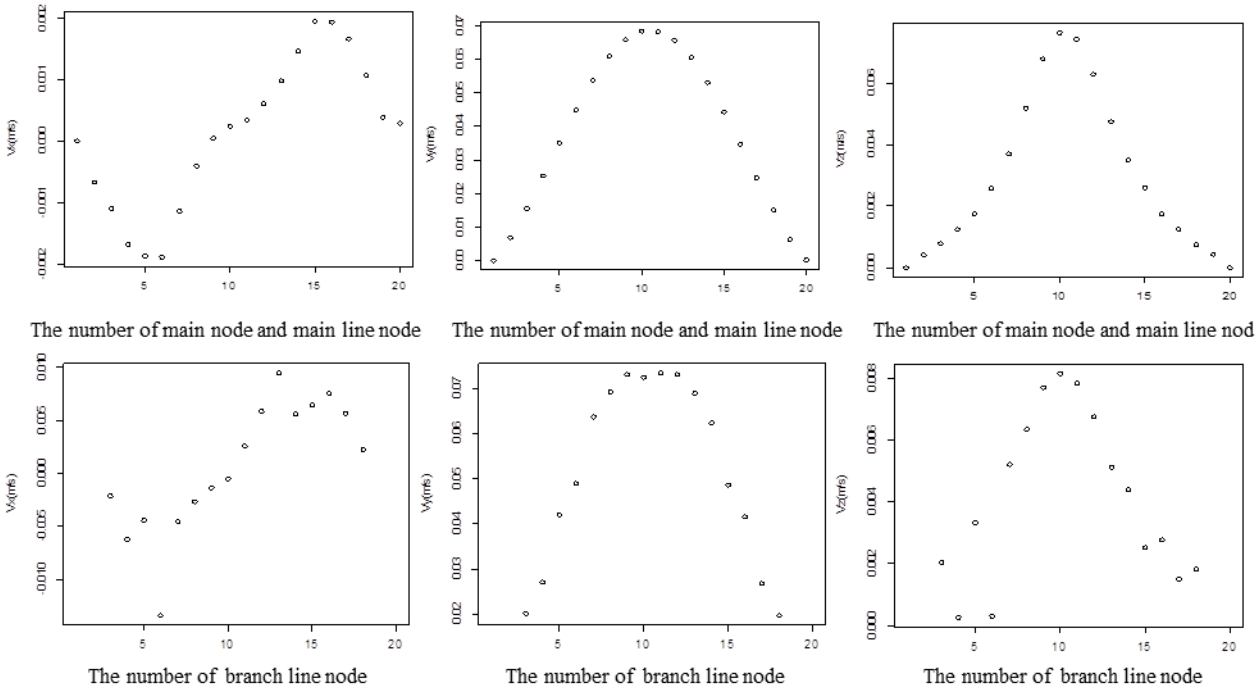
Vx(m/s)
Vy(m/s)
Vz(m/s)
The number of main node and main line node
The number of main node and main line node
The number of main node and main line nod
The number of branch line node
The number of branch line node
The number of branch line node

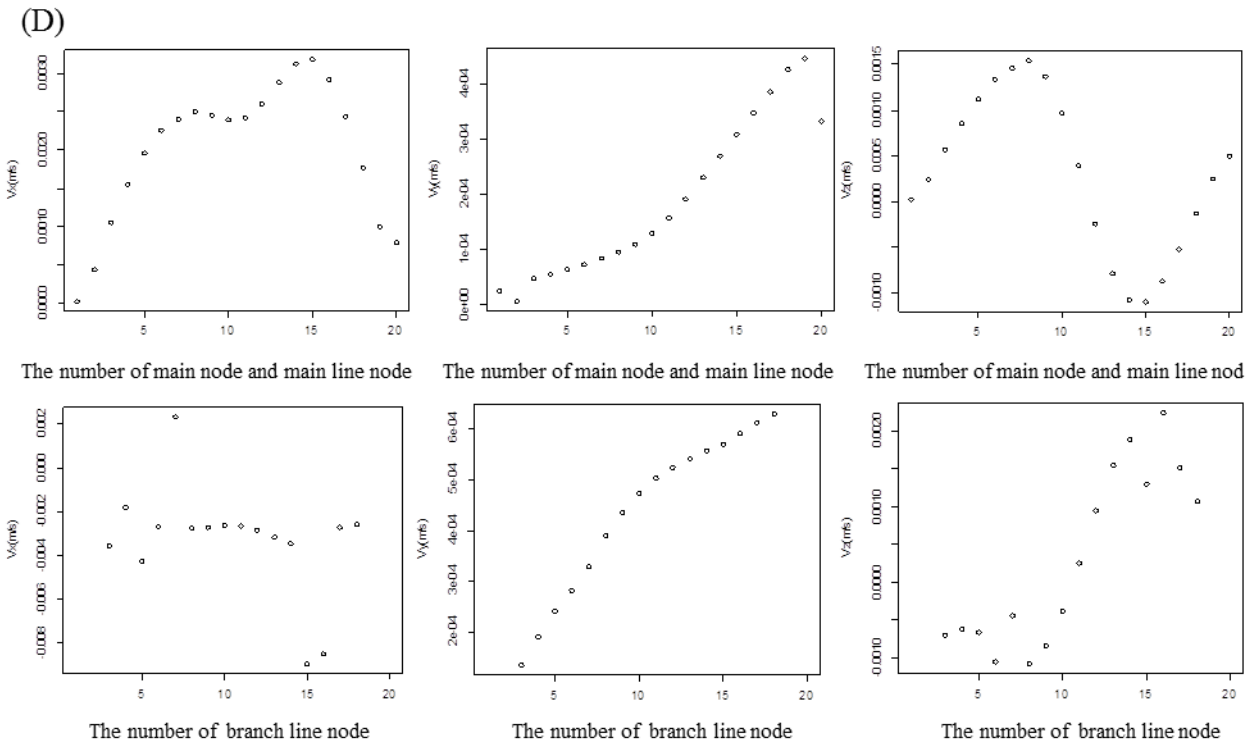

Fig.4 The initial velocity of each node in X, Y and Z axes during the retrieving process (A: Dec. 13, 2012; B: Dec. 19, 2012; C: Dec. 23, 2012; D: Dec. 31, 2012)

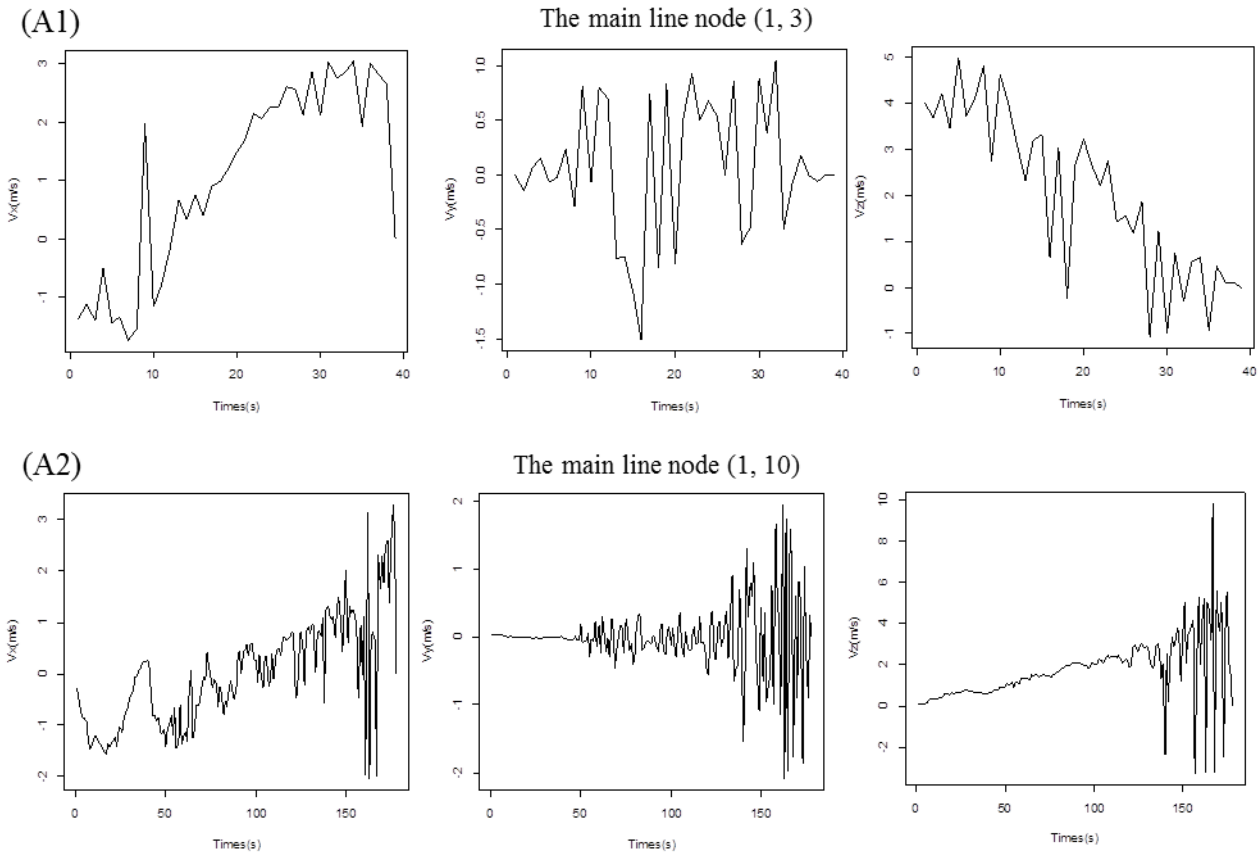

(A3) The branch line node (2, 10)

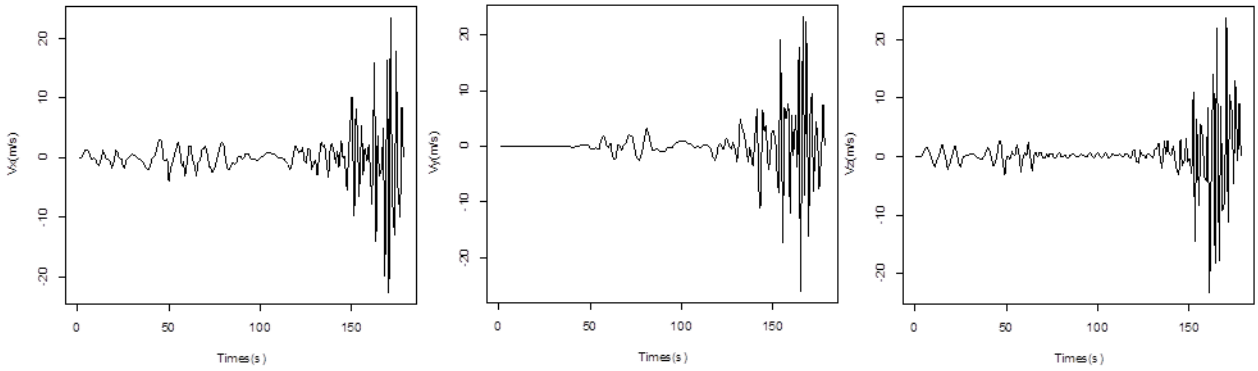

(A4) The main node (1, 19)

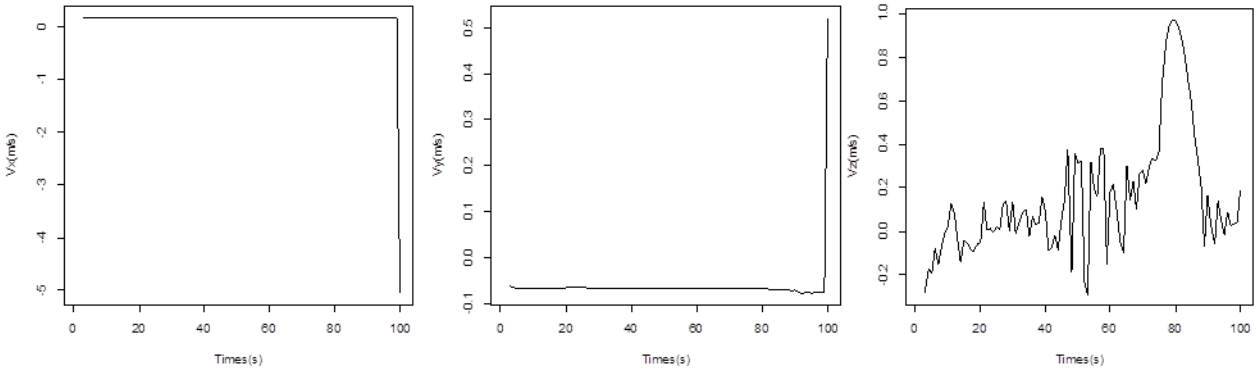

(B1) The main line node (1, 3)

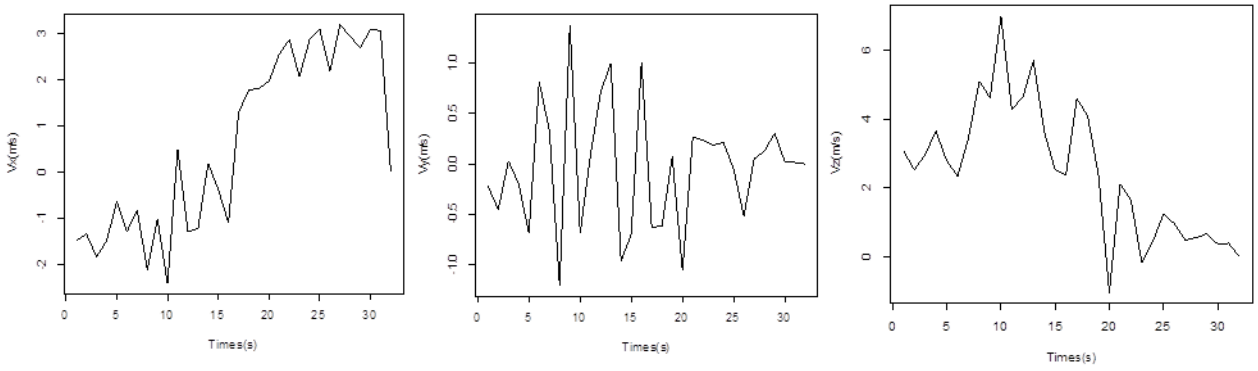

(B2) The main line node (1, 10)

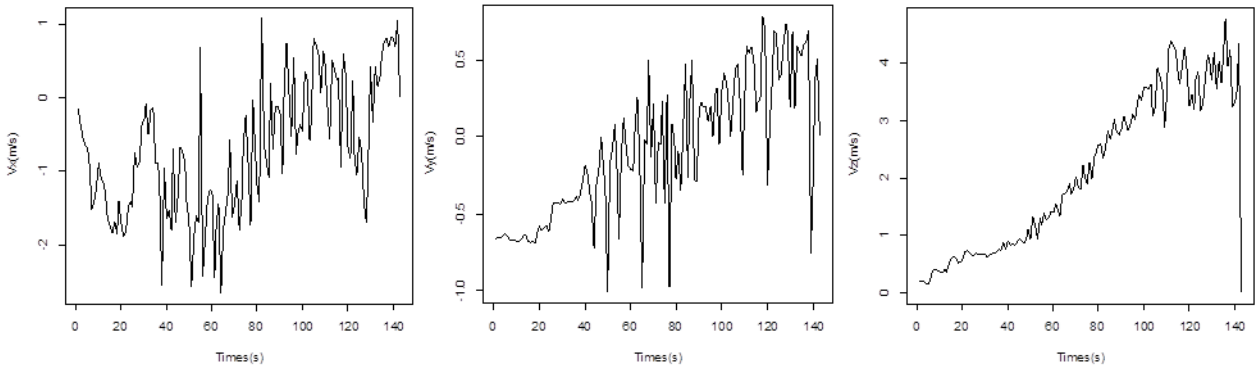

(B3) The branch line node (2, 10)

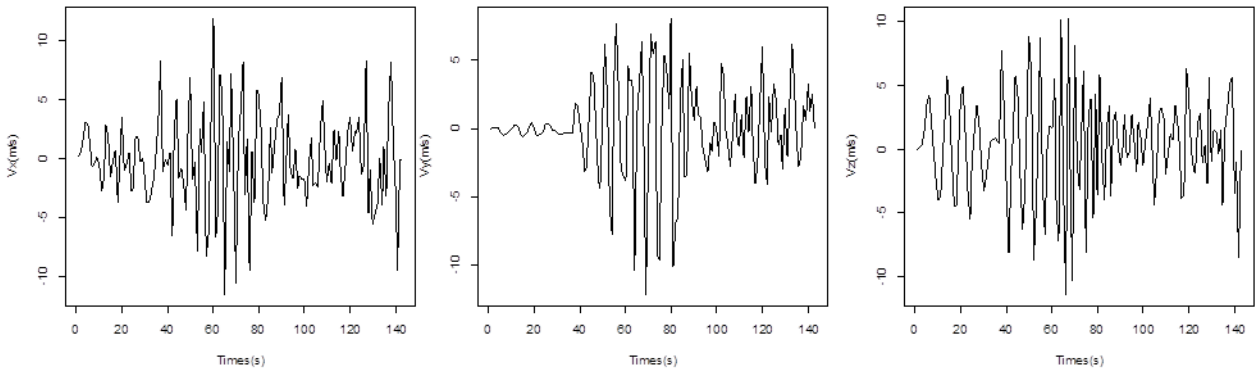

(B4) The main node (1, 19)

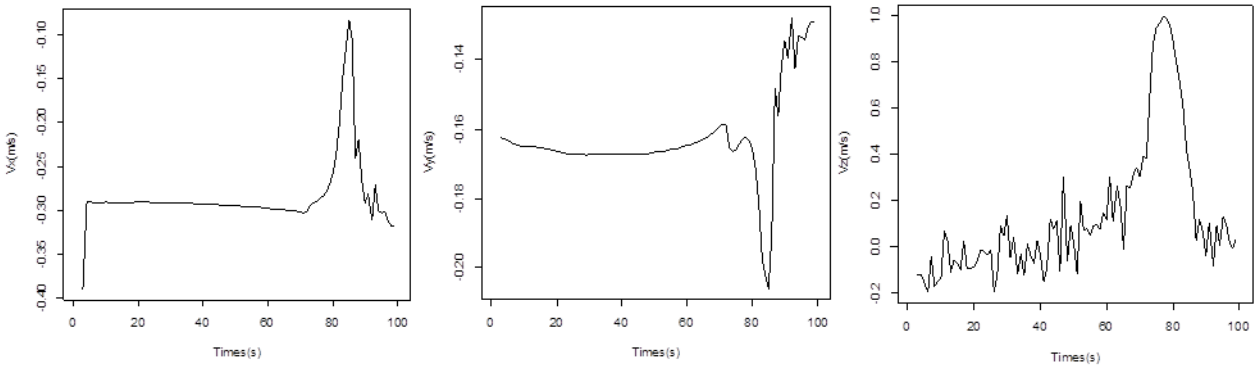

(C1) The main line node (1, 3)

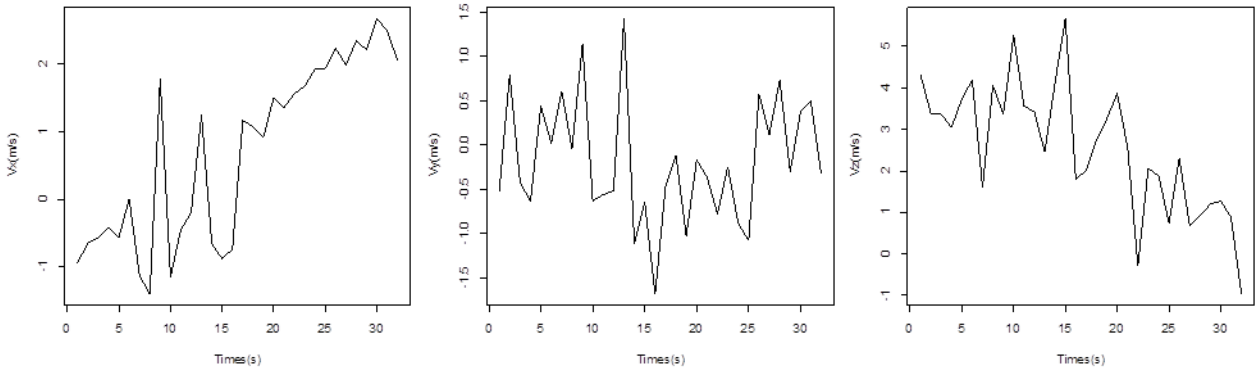

(C2) The main line node (1, 10)

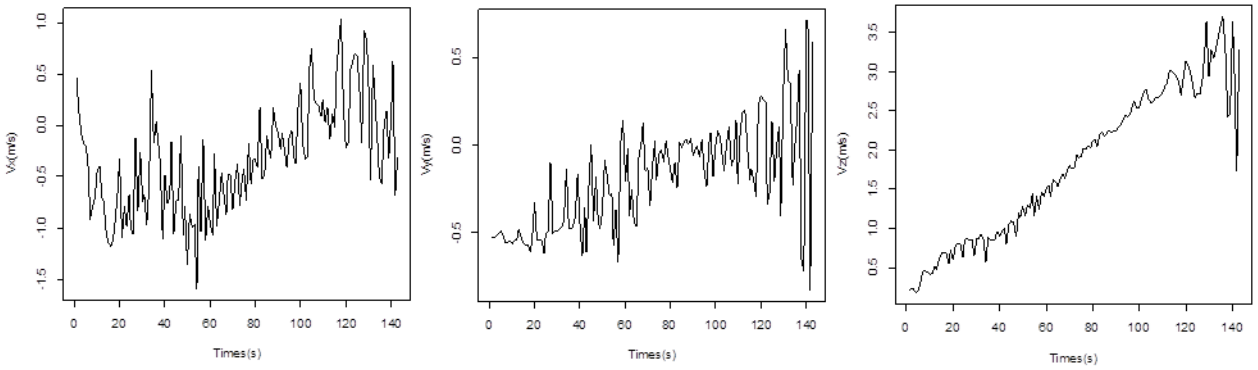

(C3) The branch line node (2, 10)

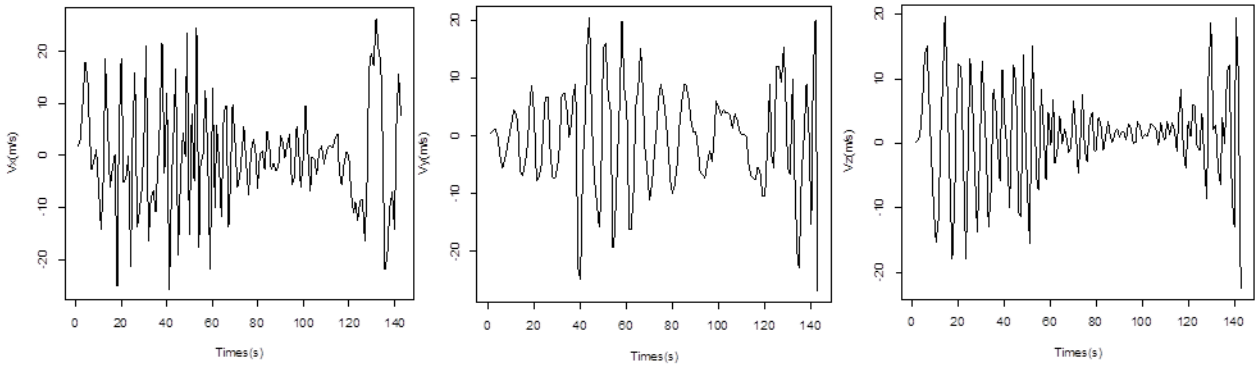

(C4) The main node (1, 19)

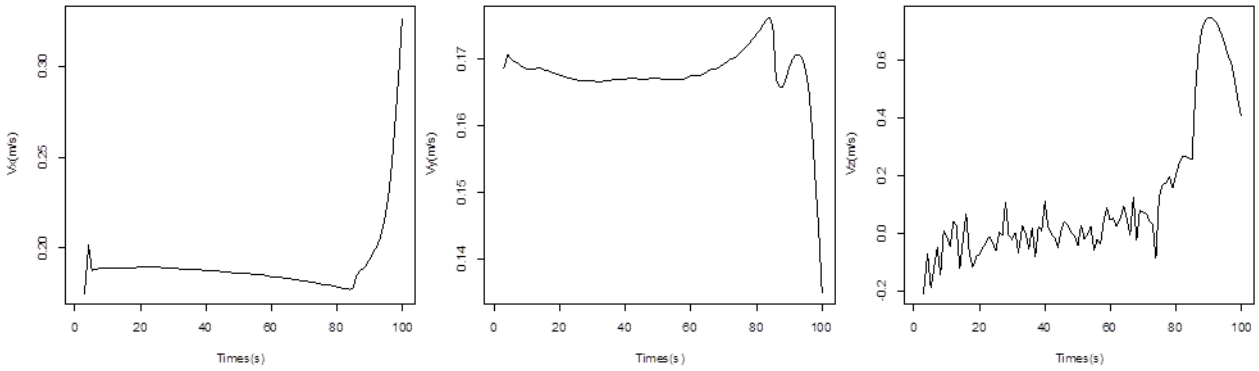

(D1) The main line node (1, 3)

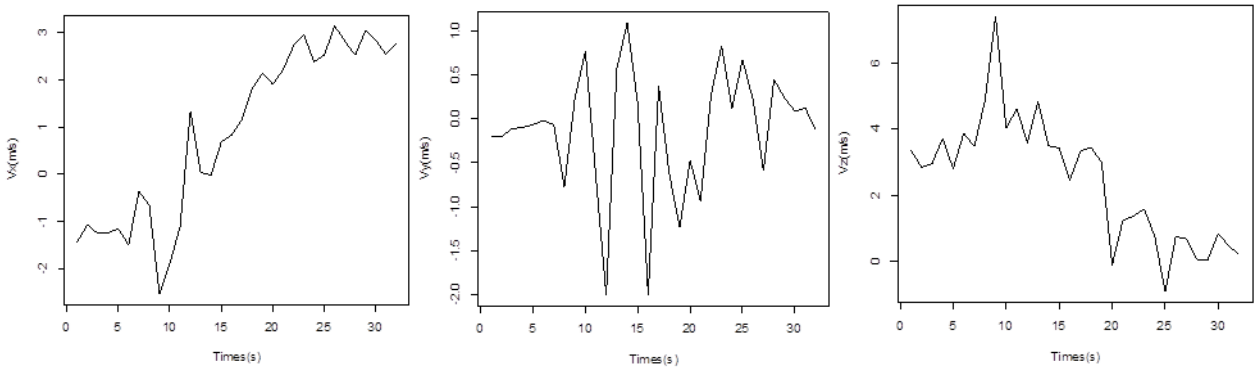

(D2) The main line node (1, 10)

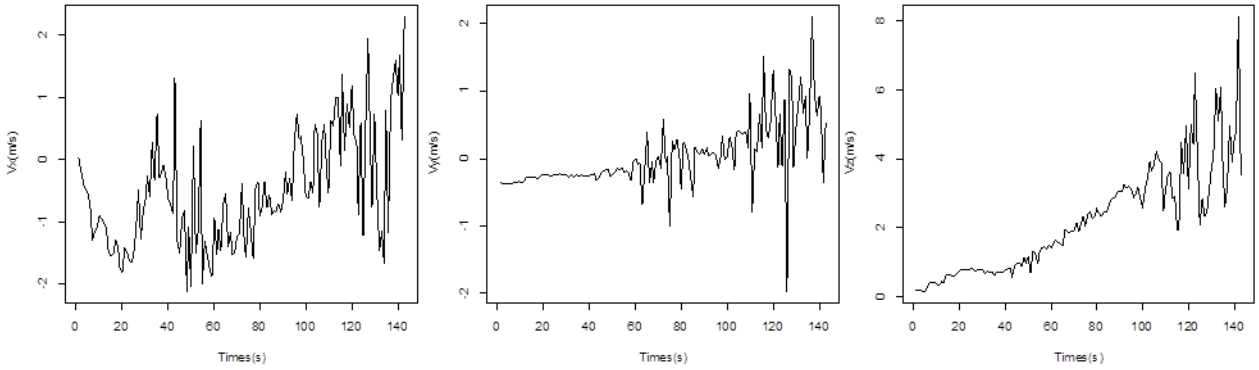

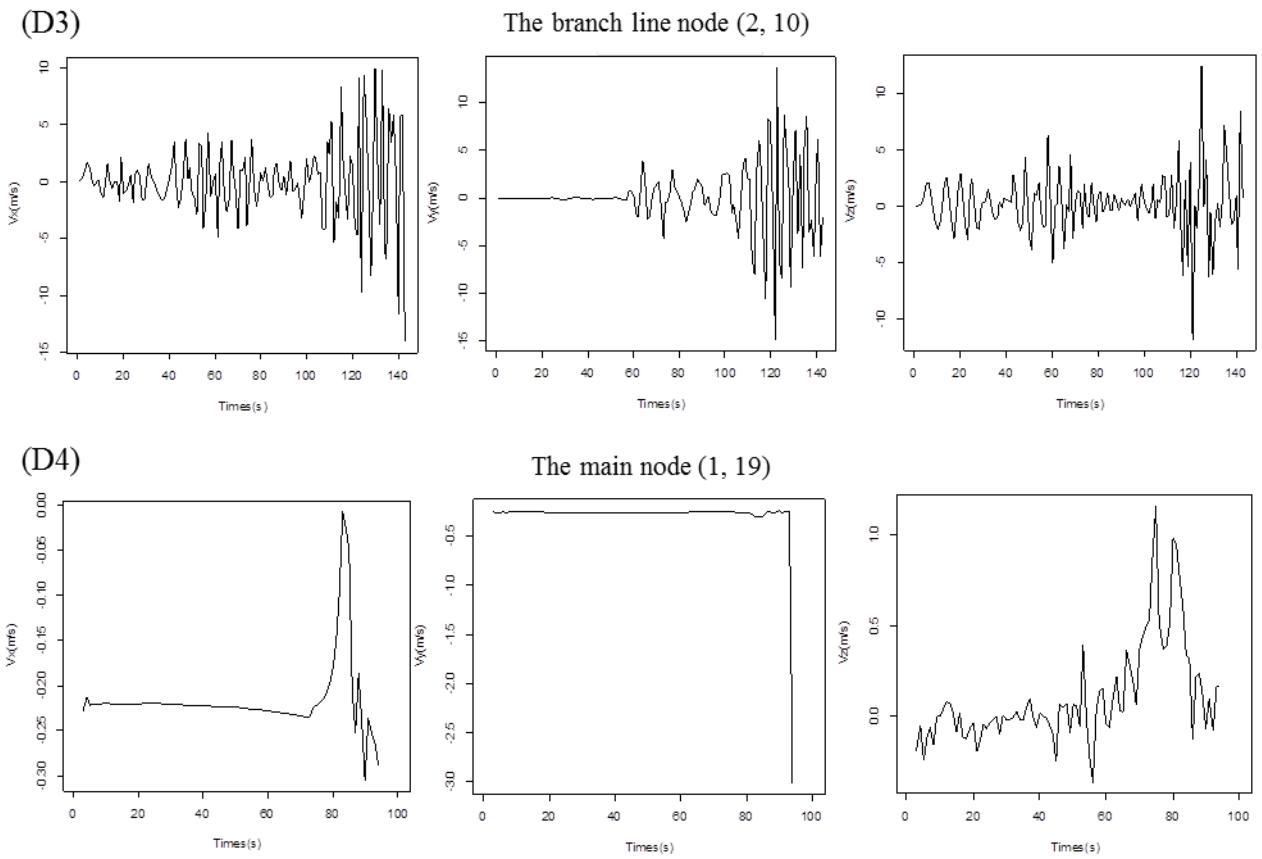

Fig.5 Velocity of the representative nodes based on the dynamic model data (A: Dec. 13, 2012; B: Dec. 19, 2012; C: Dec. 23, 2012; D: Dec. 31, 2012)

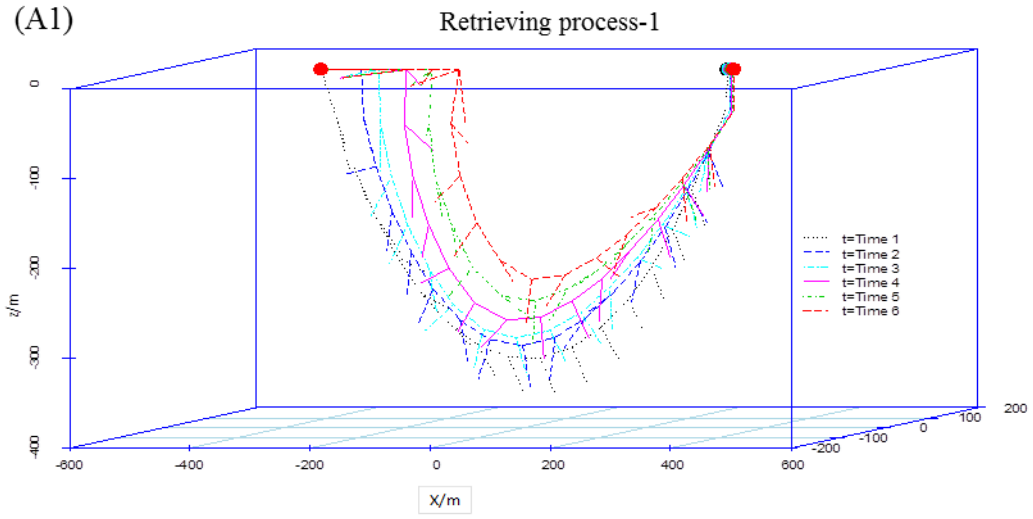

(A2) Retrieving process-2

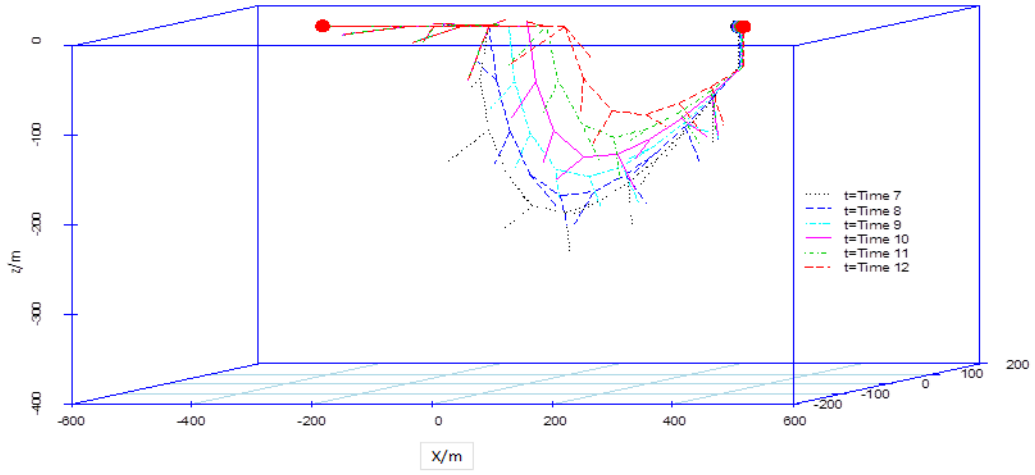

(A3) Retrieving process-3

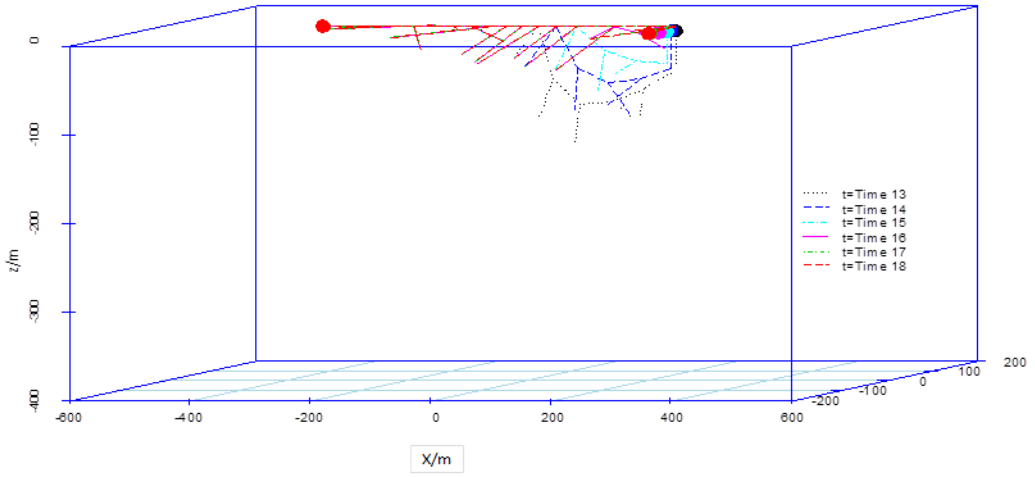

(B1) Retrieving process-1

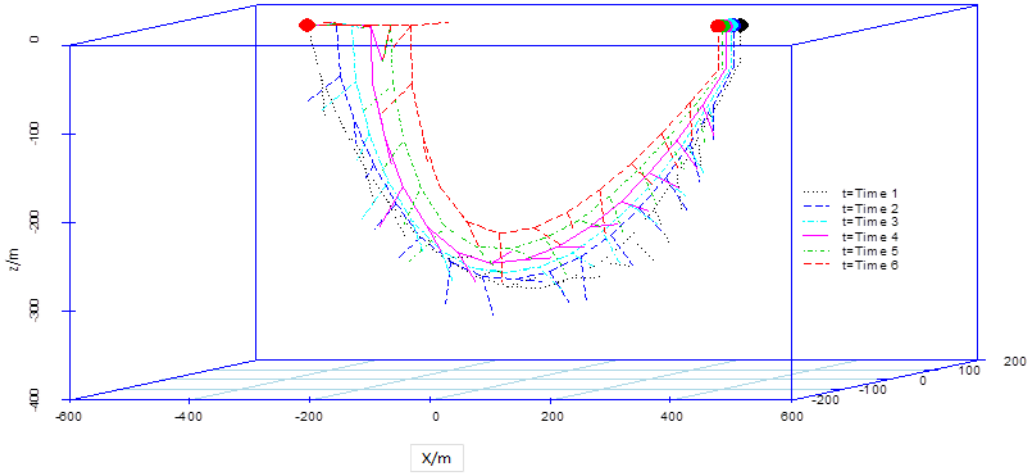

(B2) Retrieving process-2

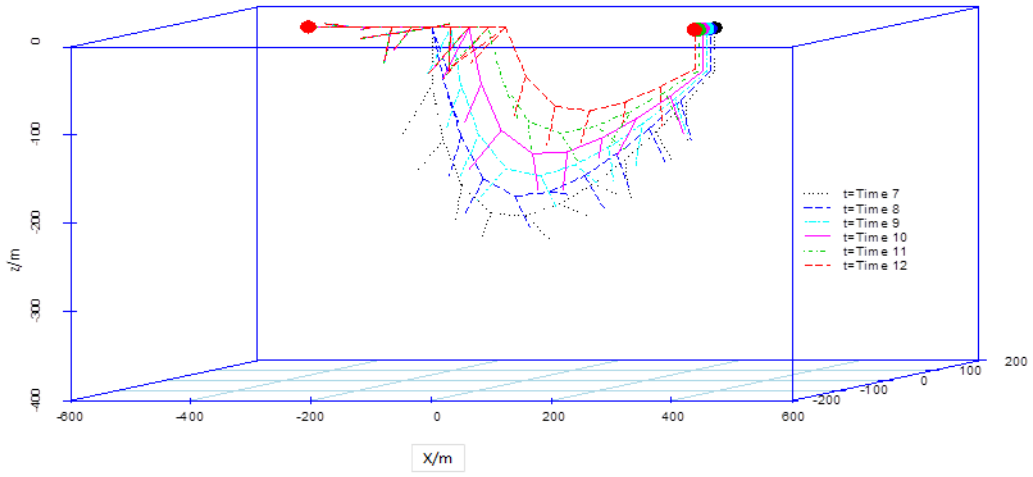

(B3) Retrieving process-3

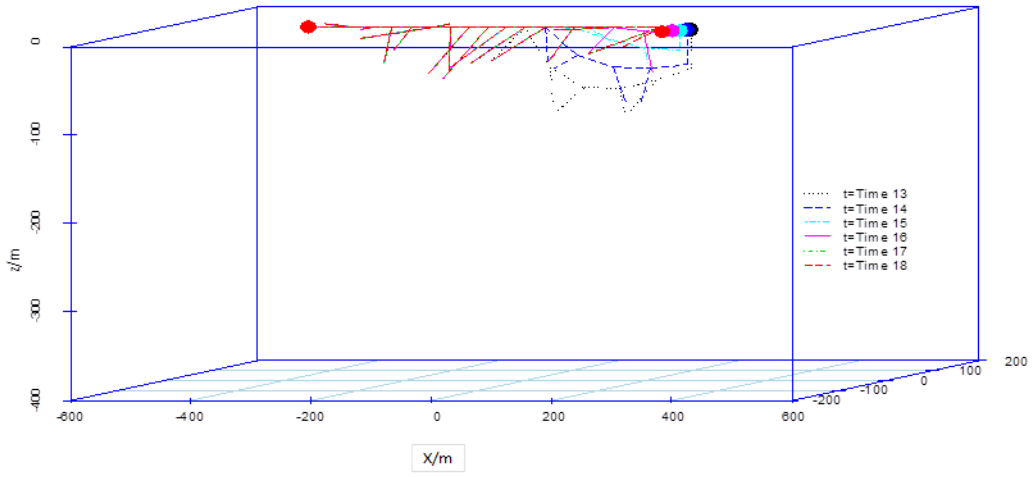

(C1) Retrieving process-1

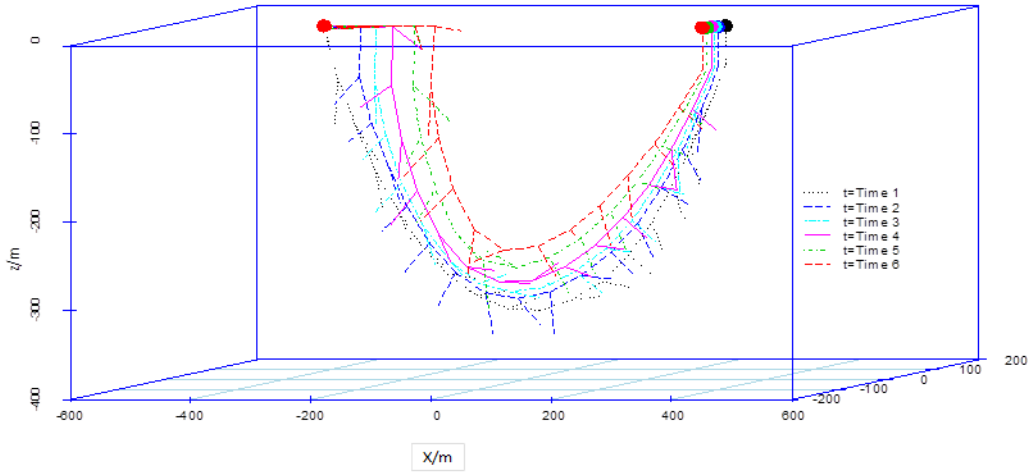

(C2) Retrieving process-2

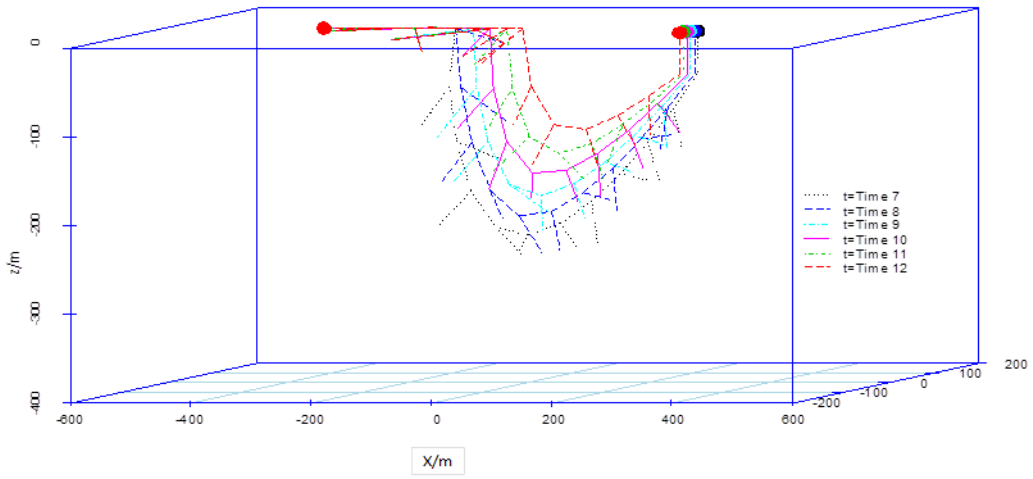

(C3) Retrieving process-3

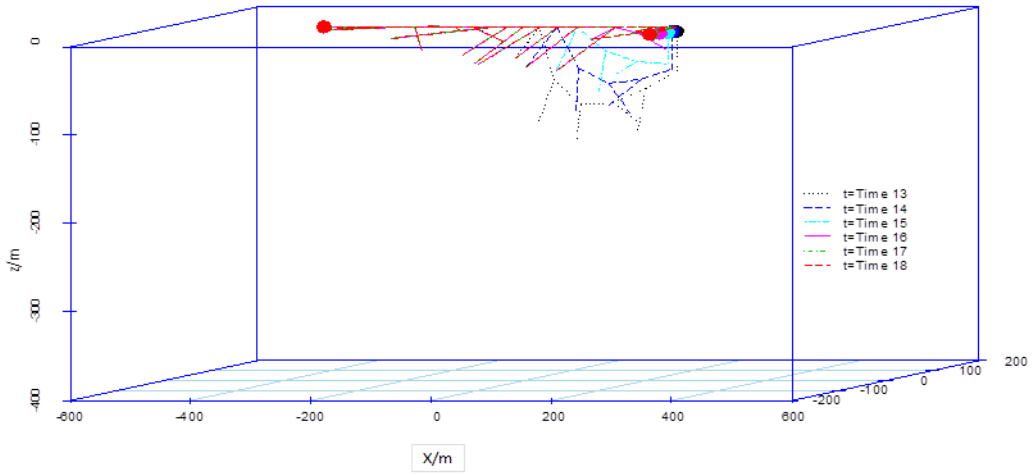

(D1) Retrieving process-1

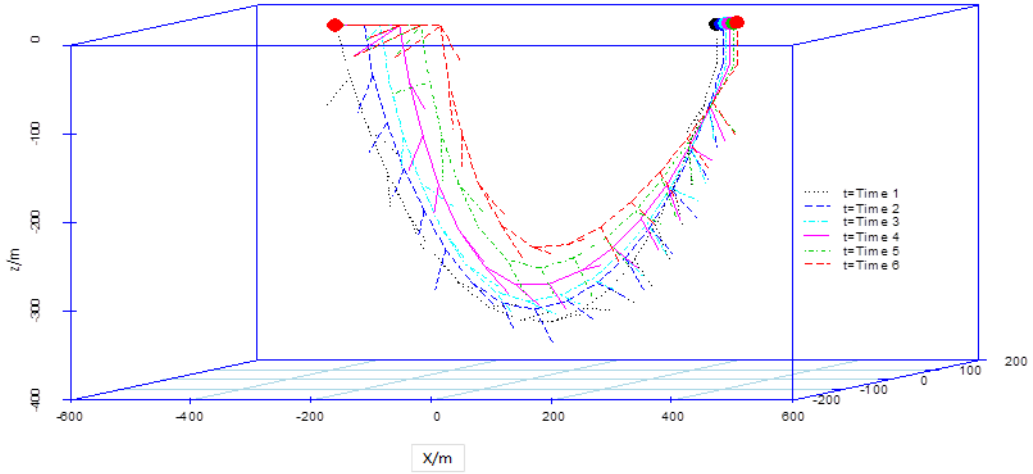

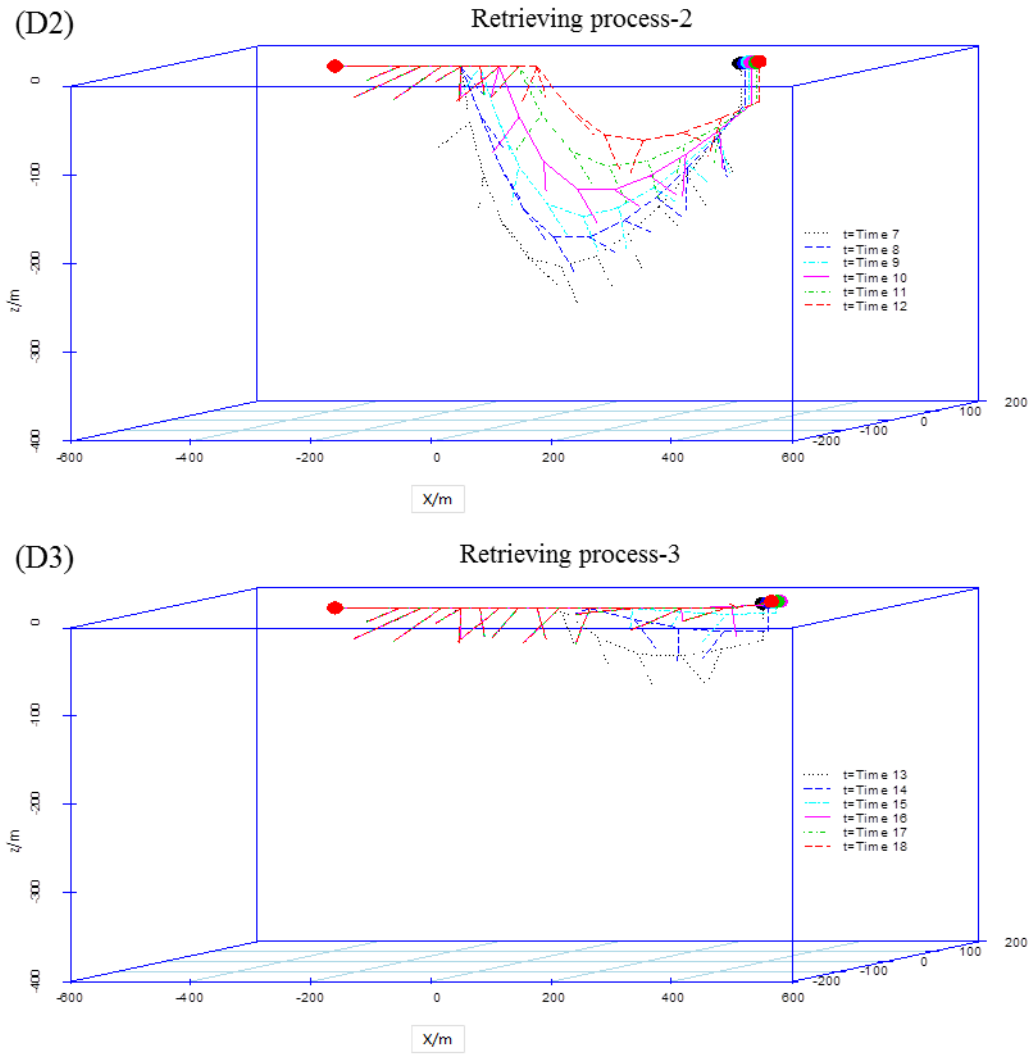

Fig.6 The retrieving simulation of longline based on the dynamic model (A: Dec. 13, 2012; B: Dec. 19, 2012; C: Dec. 23, 2012; D: Dec. 31, 2012)

(A1)

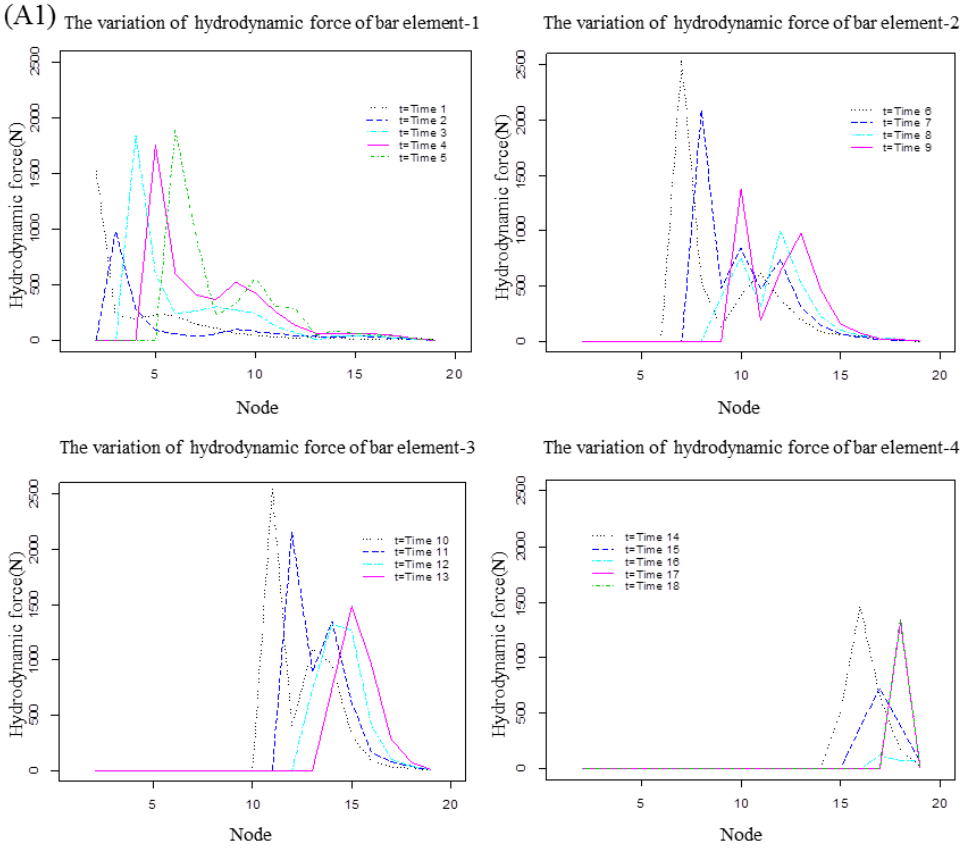
The variation of hydrodynamic force of bar element-1
Hydrodynamic force(N)
Node
t=Time 1
t=Time 2
t=Time 3
t=Time 4
t=Time 5
The variation of hydrodynamic force of bar element-2
t=Time 6
t=Time 7
t=Time 8
t=Time 9
The variation of hydrodynamic force of bar element-3
t=Time 10
t=Time 11
t=Time 12
t=Time 13
The variation of hydrodynamic force of bar element-4
t=Time 14
t=Time 15
t=Time 16
t=Time 17
t=Time 18

(A2)

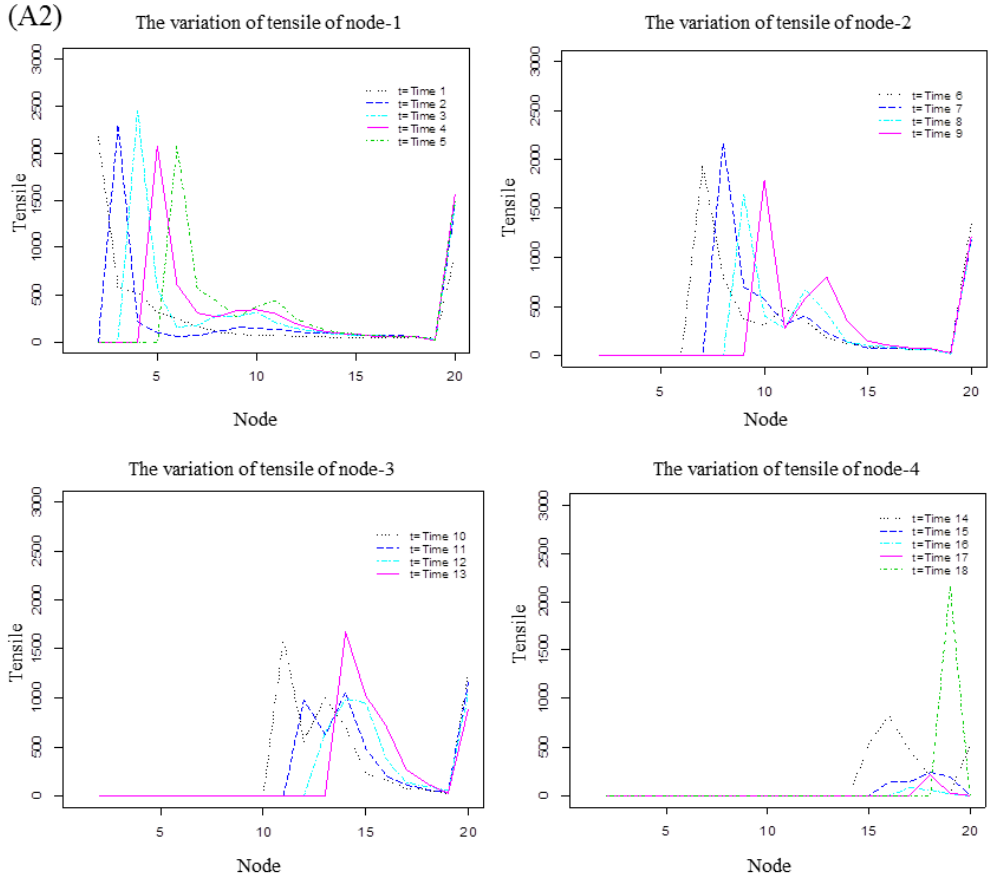
The variation of tensile of node-1
Tensile
Node
t=Time 1
t=Time 2
t=Time 3
t=Time 4
t=Time 5
The variation of tensile of node-2
t=Time 6
t=Time 7
t=Time 8
t=Time 9
The variation of tensile of node-3
t=Time 10
t=Time 11
t=Time 12
t=Time 13
The variation of tensile of node-4
t=Time 14
t=Time 15
t=Time 16
t=Time 17
t=Time 18

(B1)

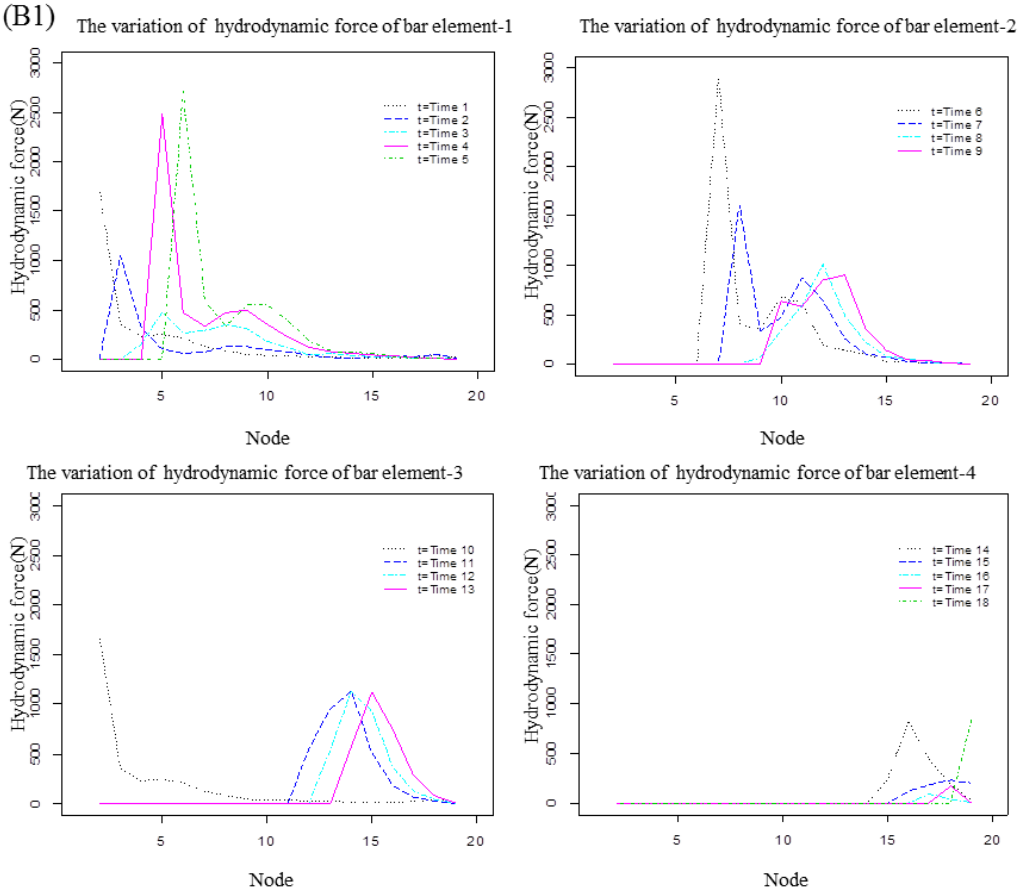
The variation of hydrodynamic force of bar element-1
Hydrodynamic force(N)
Node
t=Time 1
t=Time 2
t=Time 3
t=Time 4
t=Time 5
The variation of hydrodynamic force of bar element-2
t=Time 6
t=Time 7
t=Time 8
t=Time 9
The variation of hydrodynamic force of bar element-3
t=Time 10
t=Time 11
t=Time 12
t=Time 13
The variation of hydrodynamic force of bar element-4
t=Time 14
t=Time 15
t=Time 16
t=Time 17
t=Time 18

(B2)

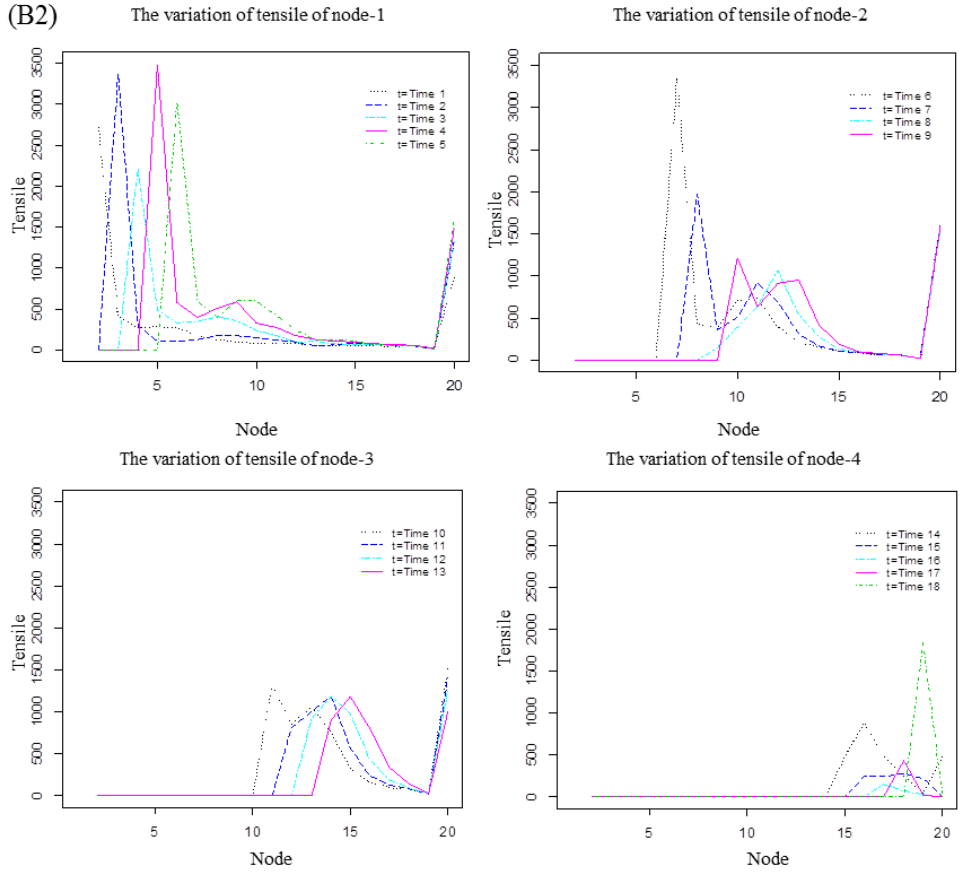
The variation of tensile of node-1
Tensile
Node
t=Time 1
t=Time 2
t=Time 3
t=Time 4
t=Time 5
The variation of tensile of node-2
t=Time 6
t=Time 7
t=Time 8
t=Time 9
The variation of tensile of node-3
t=Time 10
t=Time 11
t=Time 12
t=Time 13
The variation of tensile of node-4
t=Time 14
t=Time 15
t=Time 16
t=Time 17
t=Time 18

(C1) The variation of hydrodynamic force of bar element-1

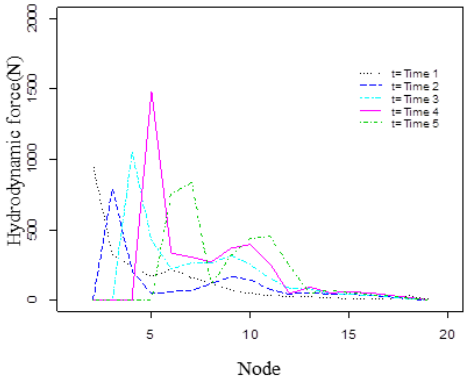

The variation of hydrodynamic force of bar element-2

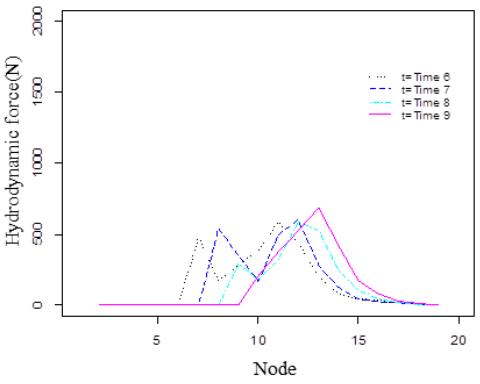

The variation of hydrodynamic force of bar element-3

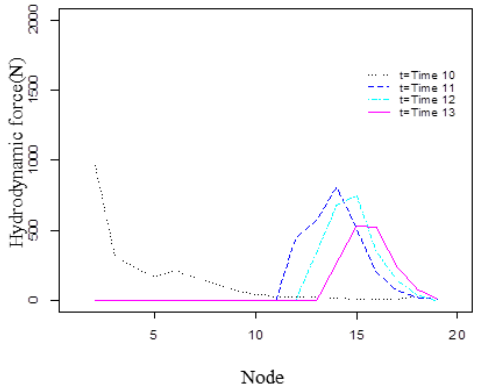

The variation of hydrodynamic force of bar element-4

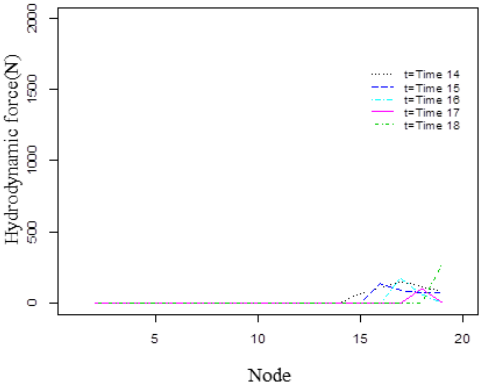

(C2) The variation of tensile of node-1

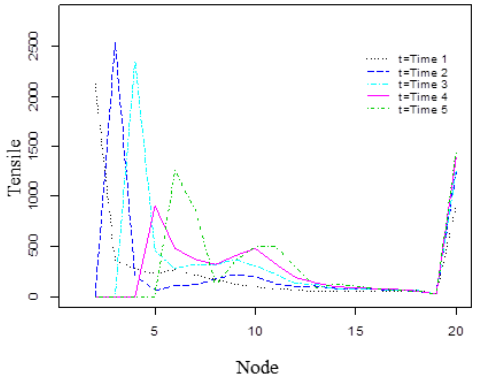

The variation of tensile of node-2

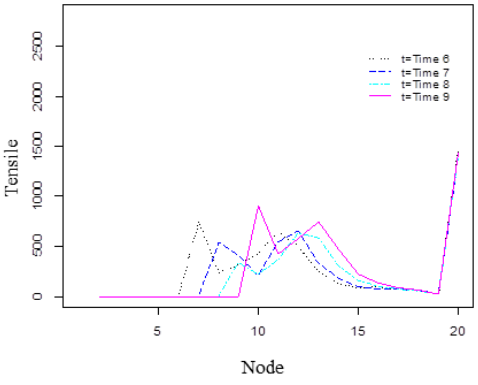

The variation of tensile of node-3

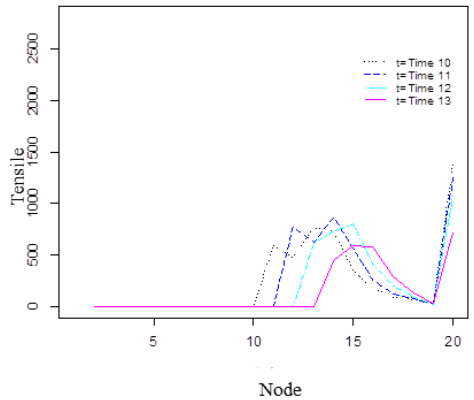

The variation of tensile of node-4

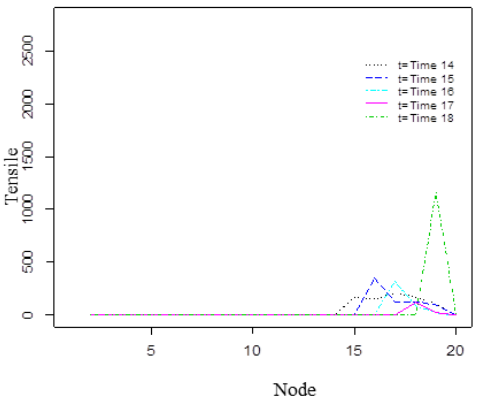

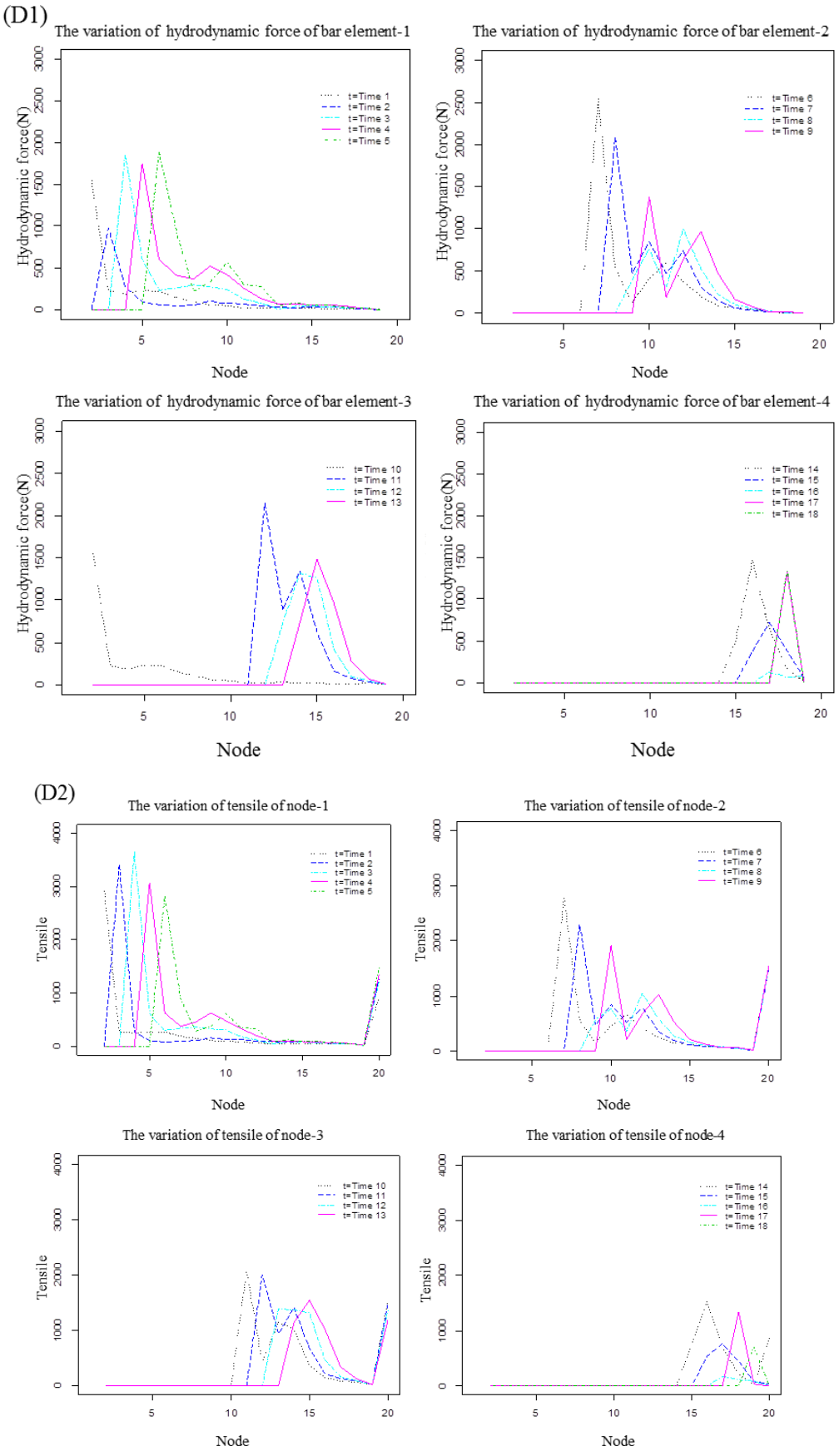

Fig.7 The variation of hydrodynamic force and tensile during the longline retrieving (A: Dec. 13, 2012; B: Dec. 19, 2012; C: Dec. 23, 2012; D: Dec. 31, 2012)

(A1)

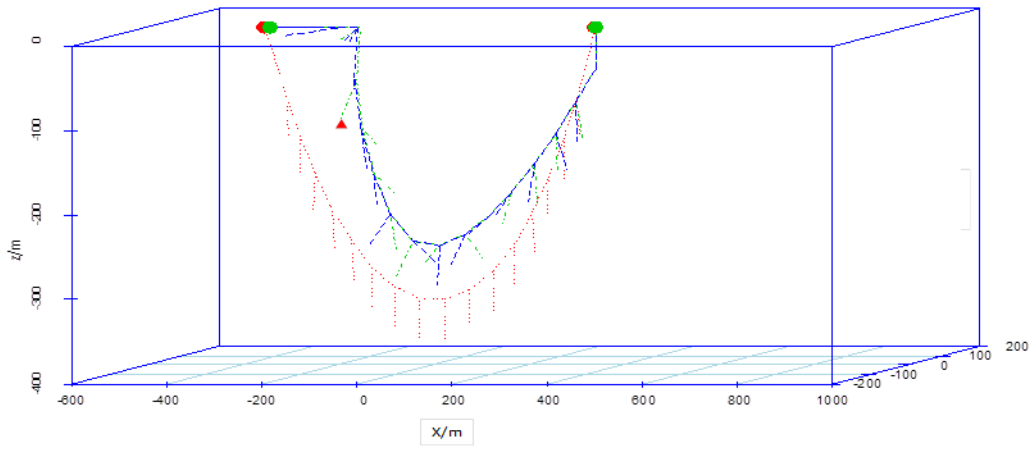

---- One individual of catch ---- No catch ▲Catches

(A2)

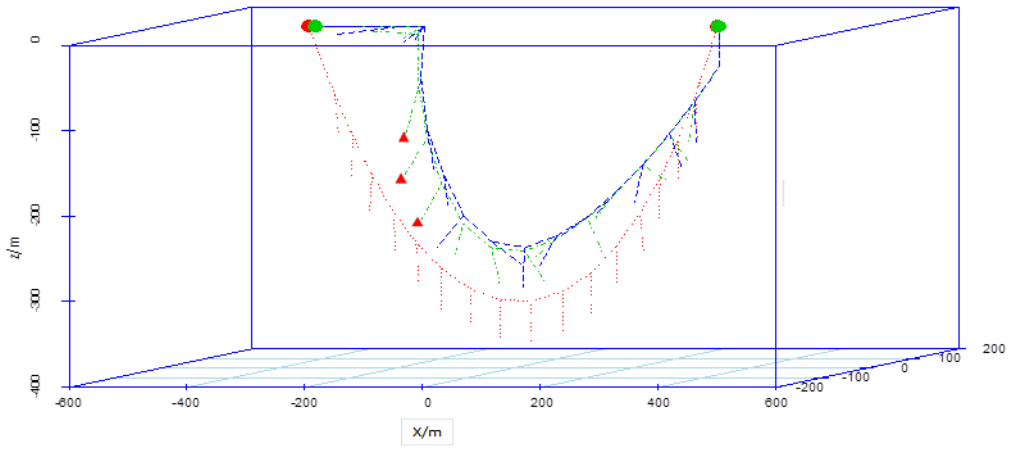

---- Three individuals of catch ---- No catch ▲Catches

(B1)

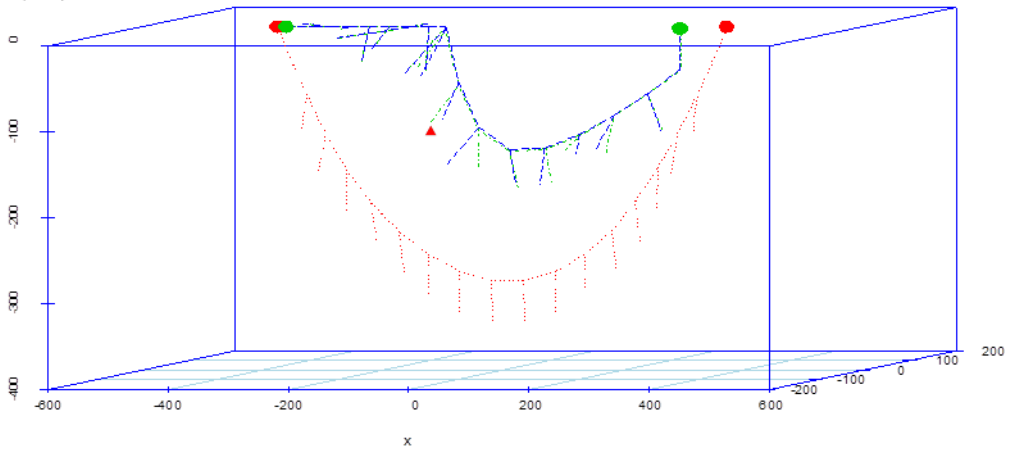

---- One individual of catch ---- No catch ▲Catches

(B2)

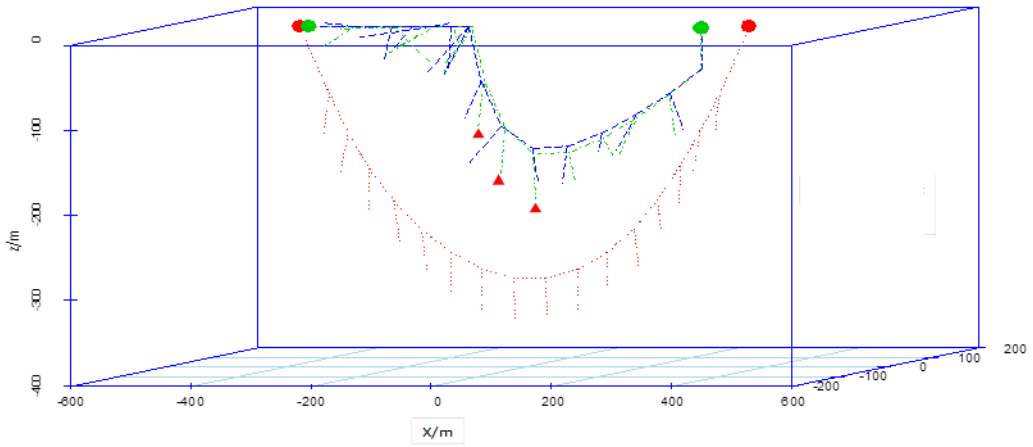

---- Three individuals of catch ---- No catch ▲Catches

(C1)

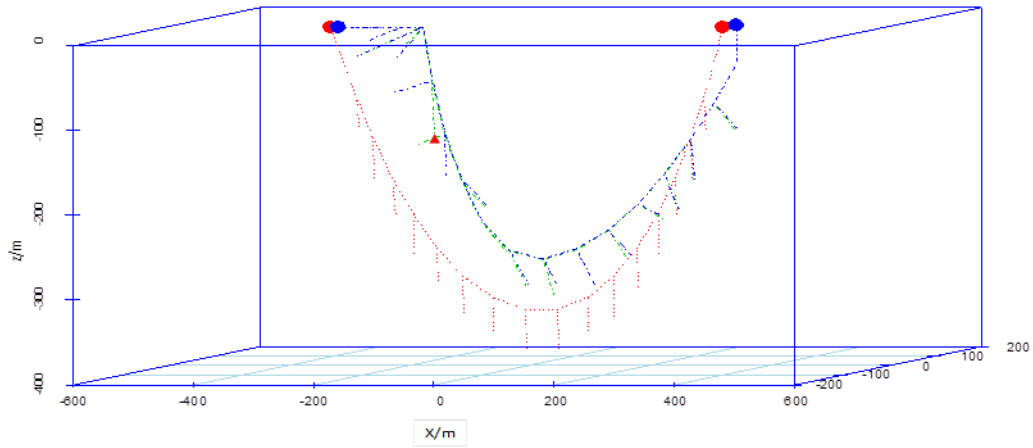

---- One individual of catch ---- No catch ▲Catches

(C2)

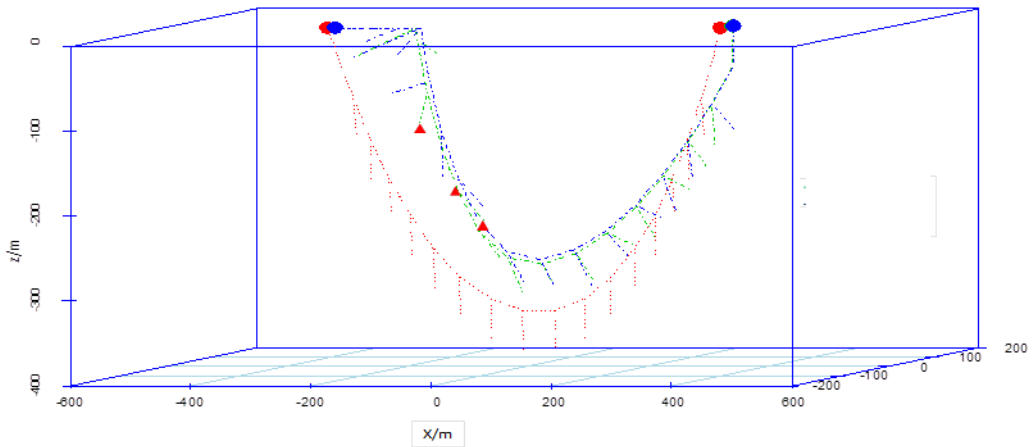

---- Three individuals of catch ---- No catch ▲Catches

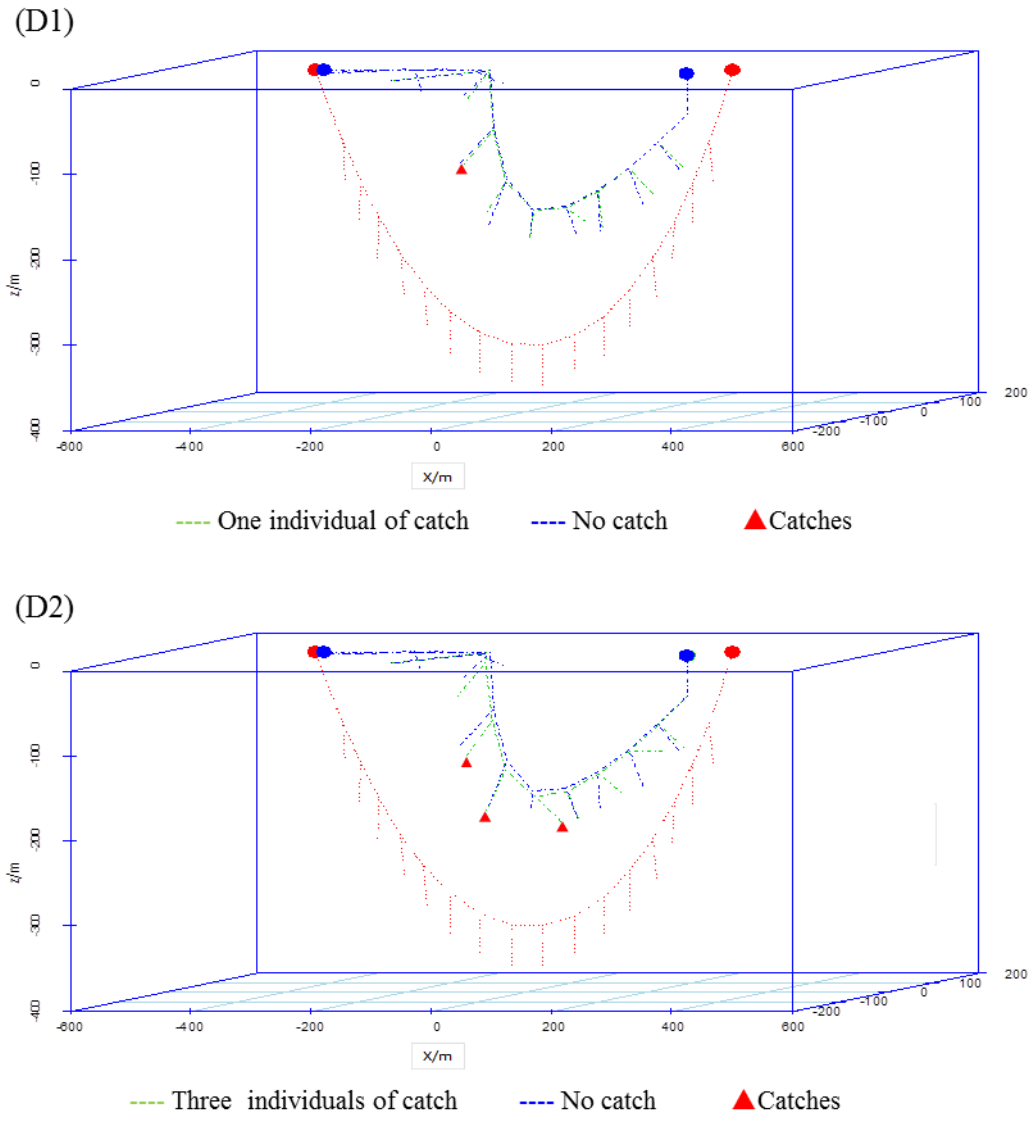

Fig.8 The impact of the catch to the retrieving process (A: Dec. 13, 2012; B: Dec. 19, 2012; C: Dec. 23, 2012; D: Dec. 31, 2012)

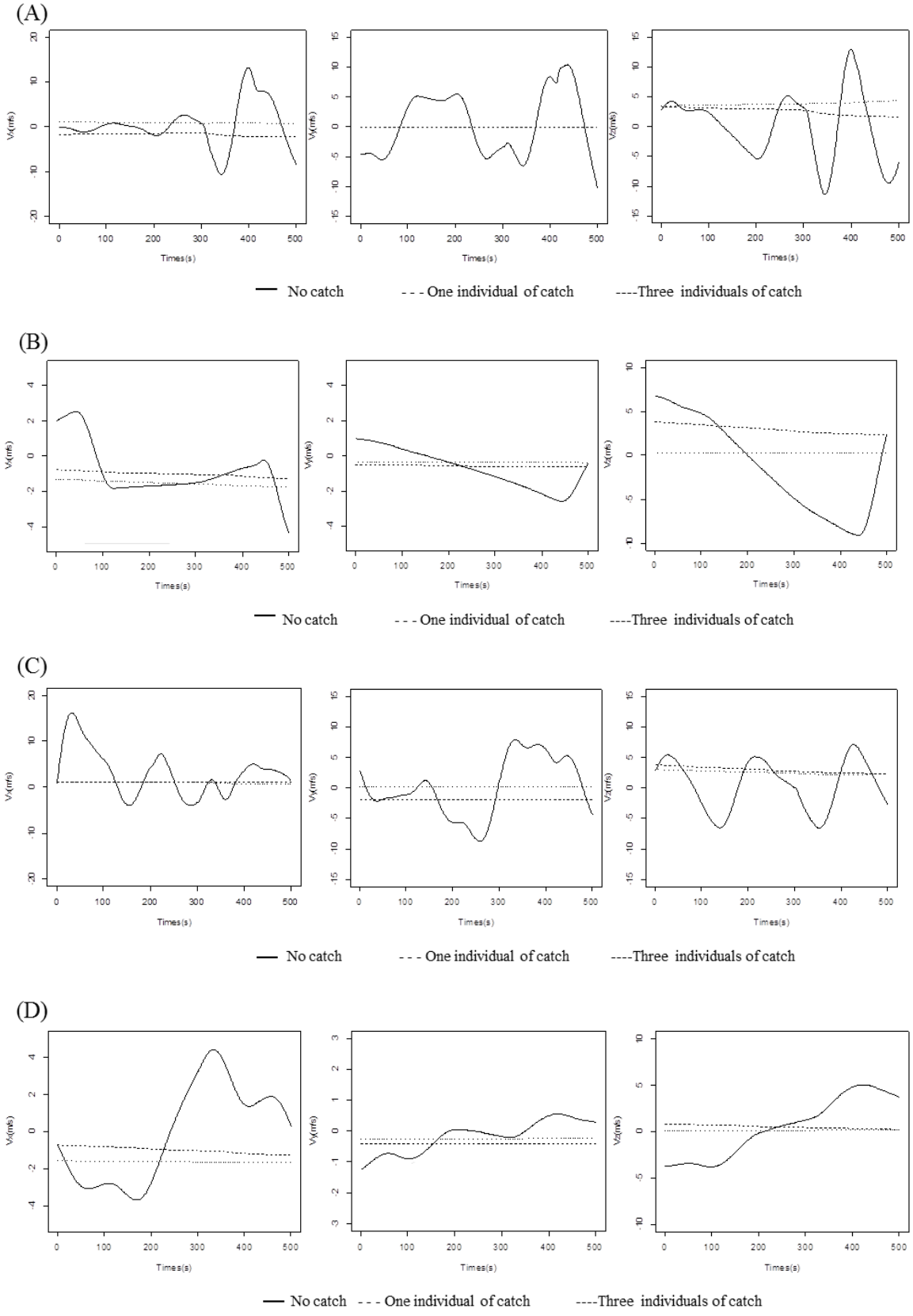

Fig.9 The impact of the catch to the movement velocity of the branch line nodes (A: Dec. 13, 2012; Dec. 19, 2012; Dec. 23, 2012; Dec. 31, 2012)

Table 1 The parameters of longline fishing gear and assumed parameter of catch

		Diameter (mm)	Material	Length (m)	L (m)	Weight in water (N)
Foat		360.00	PP	/	/	/
Float line		4.50	Nylon	35.00	/	/
Main line		6.50	Nylon Monofilament	884.34	642.22～723.44	/
Branch line	The first section	4.00	PP	2.0	/	/
	The second section	2.50	Monofilament	19.0		
	The third section	2.50	Lead centred rope	3.0		
	The fourth section	2.00	Monofilament	13.0	/	/
	The fifth section	2.50	Lead centred rope	3.0	/	/
	The sixth section	1.30	Monofilament	8	/	/
Hook and bait		/		/	/	0. 5
Catch		/		/	/	37.0

Table 2 The results of Wilcoxon rank test between the measured time (s) and the simulated time (s) of each node during the retrieving process

nodes	12.13 measured time	12.13 simulated time	12.19 measured time	12.19 simulated time	12.23 measured time	12.23 simulated time	12.31 measured time	12.31 simulated time
1,3	21.1	21.7	20.9	24.3	19.3	28.4	20.5	29.6
1,4	42.4	43.8	41.6	37.5	40	43.3	41.3	42.5
1,5	63.1	65.9	62.6	52.8	59.5	62.8	61.5	57
1,6	84.4	87.4	83.1	69.4	80. 8	83.5	81.9	75.5
1,7	105.8	110.5	104.4	86.4	100	102.8	101.7	92.5
1,8	126.2	130.2	125	102.4	119.1	122.6	122.9	109
1,9	147.6	152.6	145.1	119.1	139.9	144.8	143.5	124.3
1,10	169.2	174.3	167	134.9	160.7	163.3	164.9	139.2
1,11	190.4	196	187.1	150.3	179.3	181.7	184.6	153.1
1,12	211.1	217.5	208.8	165.5	199.3	200.4	204.8	166.8
1,13	232.4	239.3	229.1	180.7	220.7	219.6	224.8	180.4
1,14	253.3	261.6	250.6	196.2	240	240.7	246	194.1
1,15	274.5	282.8	271.2	213.3	258.3	270.1	266.3	208.7
1,16	295.5	304.9	292.1	237.4	281	298.8	287.4	225.8
1,17	316.7	326.3	312.2	270.7	298.9	327.9	307.4	257.2
1,18	337.3	348.4	334.1	307.9	320.8	351.1	327	291.5
Average time	21.1	21.8	20.9	18.9	20.1	21.5	20.4	17.8
P value	0.882		0.388		0.835		0.416	

Table.3 The velocity ranges of each representative node

nodes	Vx(m/s)		Vy(m/s)		Vz(m/s)	
	minimum	maximum	minimum	maximum	minimum	maximum
12.13-(1,3)	-1.83	3.10	-1.57	1.15	-1.08	5.11
12.13-(1,10)	-2.09	3.19	-2.12	2.05	-3.34	9.83
12.13-(2,10)	-23. 40	24. 70	-27. 80	25. 50	-23. 00	25. 10
12.13-(1,19)	-5.11	0.17	-0.07	0.53	-0.28	0.95
12.19-(1,3)	-1.58	2.71	-1.14	1.33	-1.21	6.95
12.19-(1,10)	-2.72	1.08	-1.03	0.81	0.11	4.87
12.19-(2,10)	-12.00	12.50	-13.30	8.10	-12.30	10.60
12.19-(1,19)	-0.39	0.12	-0.21	0.15	-0.21	1.02
12.23-(1,3)	-1.37	2.46	-1.62	1.50	-1.03	5.72
12.23-(1,10)	-1.58	1.04	-0.81	0.76	0.19	3.62
12.23-(2,10)	-23.70	23.10	-22.80	20.70	-21.10	20.00
12.23-(1,19)	-0.22	0.35	0.14	0.18	-0.22	0.73
12.31-(1,3)	-2.38	3.07	-2.03	1.07	-0.87	7.12
12.31-(1,10)	-2.09	2.14	-2.02	2.03	0.07	8.13
12.31-(2,10)	-14.60	10.8	-15.30	13.10	-11.70	12.50
12.31-(1,19)	-0.30	0.01	-3.07	-0.34	-0.36	1.23

Table.4 The range of tension and hydrodynamic force of each node

Date	Tension (N)		Hydrodynamic force (N)	
	minimum	maximum	minimum	maximum
12.13	0	2481	0	2053
12.19	0	3537	0	2890
12.23	0	2575	0	1491
12.31	0	3647	0	2544

Reference

Bigelow, K. A., Hampton, J., Miyabe, N., 2002. Application of a habitat-based model to estimate effective longline fishing effort and relative abundance of Pacific bigeye tuna (*Thunnus obesus*). Fish. Oceanogr. 11, 143-155.

Bigelowa, K., Musyl, M. K., Poisson, F., Kleiber, P., 2006. Pelagic longline gear depth and shoaling. Fish. Res. 77, 173-183.

Boggs, C. H., 1992. Depth, capture time, and hooked longevity of longline caught pelagic fish: timing bites of fish with chips. Fish. Bull. 90, 642-658.

Cao, D. M., 2011. The dynamic simulation of tuna longline. Shanghai Ocean University, Shanghai (in Chinese, with English abstract).

Cao, D.M., Song, L.M., Li, J., Yuan, J.T., Zhou, Y.Q., 2014. Determining the drag coefficient of a cylinder perpendicular to water flow by numerical simulation and field measurement. Ocean Eng. 85, 93–99.

Jiang, L.B., Xu, L.X., Huang, J.L., 2005. Relationship between vertical distribution of bigeye tuna (*Thunnus obesus*) and water temperature in Indian Ocean. J. Shanghai fish. Univ. 14(3), 333-336 (in Chinese, with English abstract).

Johansen, V., 2007. Modelling of Flexible Slender Systems for Real-time Simulation and Control Applications. Marine Engineering, NTNU.

Lee, J. H., Lee, C.W., Cha, B.J., 2005. Dynamic simulation of tuna longline gear using numerical methods. Fish. Sci. 71,1287–1294.

Mizuno, K., Okazaki, M., Miyabe, N., 1998. Fluctuation of longline shortening rate and its effect on underwater longline shape. Bull. Nat. Res. Inst. Far Seas Fish. 35,155-164.

Mizuno, K., Okazaki, M., Nakano, H., Okamura, H., 1999. Estimation of underwater shape of tuna longline with micro-bathythermographs. Int. Am. Trop. Tuna Commun. Spec. Rep. 10, 35.

Miyamoto, Y., Uchida, K., Orii, R., Wen, Z., Shiode, D., Kakihara, T., 2006. Three-dimensional underwater shape measurement of tuna longline using ultrasonic positioning system and ORBCOMM buoy. Fish. Sci. 72, 63–68.

Nakano, H., Okazaki M., Okamoto, H., 1997. Analysis of catch depth by species for tuna longline fishery based on catch by branch lines. Bull. Nat. Res. Inst. Far. Seas. Fish. 34, 43-62.

Song, L.M., Chen, X.J., Xu, L.X., 2004. Relationship between bigeye tuna vertical distribution and the temperature, salinity in the Central Atlantic Ocean. J. Fish. Sci. China 11(6), 561-566 (in Chinese, with English abstract).

Song, L.M., Gao, P.F., 2006. Captured depth, water-temperature and salinity of bigeye tuna (*Thunnus obesus*) longlining in Maldives waters. J. fish. China 30(3), 335-340 (in Chinese, with English abstract).

Song, L.M., Zhang, Y., Xu, L.X., Jiang, W.X., Wang, J.Q., 2008. Environmental preferences of longlining for yellowfin tuna (*Thunnus albacares*) in the tropical high seas of the Indian Ocean. Fish. Oceanogr. 17(4),239-253.

Song, L.M., 2008. Habitat environment integration index of bigeye tuna (*Thunnus obesus*) in the Indian Ocean-Based on longline survey data. Shanghai Ocean University, Shanghai, (in Chinese, with English abstract).

Song, L.M., Zhang, Z., Yuan, J.T., Li, Y.W., 2011. Numeric modeling of the pelagic longline based on the finite element analysis. Oceanologia et limnologia sinica, 42(2), 256-261(in Chinese, with English abstract).

Song, L.M., Zhang, Z., Yuan, J.T., Li, Y.W., 2011. Numeric modeling of a pelagic longline based on minimum potential energy principle． J. Fish. Sci. China 18(5), 1170-1178 (in Chinese, with English abstract)．

Song, L.M., Li, J., Gao, P.F., Zhou, J., Xu, L.X., 2012. Modeling the hook depth distribution of pelagic longlining in the equatorial area of Indian Ocean. J. Ocean Univ. China 11 (4), 547-556.

Song, L.M., Li, J., Xu, W.Y., Zhang, X.F., 2015. The dynamic simulation of the pelagic longline deployment. Fish. Res. 167,280-292.

Song, L.M., 2015. Environmental biology of fishes and gear performance in the pelagic tuna longline fishery. Science press, Beijing.

Suzuki, Z., Warashina,Y., Kishida, M., 1977. The comparison of catches by regular and deep tuna longline gears in the western and central equatorial Pacific. Bull. Far. Seas. Fish. Res. Lab. 15,51-89.

Walton, T., Polachek, H., 1960. Calculation of transient motion of submerged cables. Math. Comput. 14 (69), 27–46.

Wan, R., Hu, F.X., Tokai, T., Matuda, K., 2002. A method for analyzing the static response of submerged rope systems based on a finite element method. Fish. Sci. 68, 65–70.

Wan, R., Cui, J.H, Song, X.F., Tang, Y.L., Zhao, F.F., Huang, L.Y., 2005. A numerical model for predicting the fishing operation status of tuna longline. J. fish. China 29 (2), 238-245 (in Chinese, with English abstract).

Wilcoxon, F., 1945. Individual comparisons by ranking methods. Biometric Bull. 1(6), 80~83.

Wu, Y.W., Wu, Y.S., 2005. The application of catenary and parabola theories in tuna longline fishery. Mar. Fish. 27(1), 1-9.

Yao, Y.M., Chen, Y.L., Zhou, H., Yang, H.Y., 2016. A method for improving the simulation efficiency of trawl based on simulation stability criterion. Ocean Eng. 117, 63–77.

Zhang, X.F., Cao, D.M, Song, L.M., Zou, X.R., Chen, X.J., Xu, L.X., Zhang, M., Zhang, J., Zhou, Y.Q., 2012. Application of whole—implicit algorithm and virtual neural lattice in pelagic longline modeling. 2012 9th International Conference on Fuzzy Systems and Knowledge Discovery (FSKD 2012), May 29-31, 2012, Chongqing, China, 9, 2616-2619.

Zhou, Y. Q., Xu, L. X., He, Q. Y., 2001. The Dynamics of Fishing Gear. China Agricultural Press, Beijing (in Chinese).